

SPIN NERNST & SPIN HALL EFFECT IN DILUTE METALLIC ALLOYS

Dissertation

zur Erlangung des akademischen Grades
doctor rerum naturalium (Dr. rer. nat.)

vorgelegt

von **Katarina Tauber**

geb. am 06.11.1984 in Halle

Institut für Physik
der Naturwissenschaftlichen Fakultät II
der Martin-Luther-Universität Halle-Wittenberg



Halle, December 13, 2013

Erstgutachterin: Prof. Dr. Ingrid Mertig
Zweitgutachter: Prof. Dr. Steffen Trimper
Drittgutachter: Prof. Dr. Peter Kratzer

Tag der öffentlichen Verteidigung: 18.06.2014

*To my grandfather Karl,
who handed me down probably most of my talents,
but never had the chance to share their fruits with me.*

“On the infrequent occasions when I have been called upon in a formal place to play the bongo drums, the introducer never seems to find it necessary to mention that I also do theoretical physics.”

R. FEYNMAN

On the infrequent occasions when I struggle with my life as a physicist I tend to recollect Feynman’s stories, where I recognize my own nature - although probably no one else can see the similarities. However, I truly believe they exist and help me feeling rooted in who I am. I then remember that a scientist is what I am supposed to and one of the personalities I always wanted to be, but apart from that have anytime the choice to be anybody else.

K. TAUBER

ABSTRACT

This work includes ab initio studies of two transverse spin transport phenomena, namely, the spin HALL and spin NERNST effect. These effects refer to the appearance of a transverse spin accumulation or spin current due to a longitudinal electrical field or temperature gradient, respectively.

Dilute alloys composed of a Cu host with substitutional impurities are studied. A special focus is set on the behaviour of dilute ternary alloys to discover, if two types of impurities acting in combination can enhance the efficiency of the above mentioned phenomena.

For the electronic structure calculations performed within the density functional theory a relativistic screened KORRINGA-KOHN-ROSTOKER method is used. The transport properties of the considered systems are obtained via the BOLTZMANN approach.

CONTENTS

1	INTRODUCTION	11
2	TRANSVERSE SPIN TRANSPORT PHENOMENA	15
2.1	Classification	15
2.2	Observation	16
2.3	Mechanisms	17
3	METHODS	21
3.1	Electronic structure	21
3.1.1	Density functional theory	21
3.1.2	KKR - a GREEN function method	24
3.1.3	Relativistic KKR method	26
3.2	Electronic transport	38
3.2.1	BOLTZMANN approach	38
3.2.2	Transport properties	40
3.2.3	Spin HALL effect	44
3.2.4	Spin NERNST effect	45
3.2.5	Ternary alloys - MATTHIESSEN's rule	49
3.3	Technical remarks	54
3.3.1	Transport KKR code for ternary alloys	54
3.3.2	Integration over the energy	54
4	RESULTS	57
4.1	Spin NERNST effect in binary alloys	57
4.1.1	Open circuit case	58
4.1.2	Short circuit case	61

4.2	Influence of spin-flip scattering and the accuracy of the Fermi surface integration	67
4.3	Validity of MATTHIESSEN's rule for the longitudinal resistivity & HALL resistivity	71
4.4	Spin HALL & spin NERNST effect in ternary alloys	75
4.4.1	Spin HALL effect	75
4.4.2	Spin NERNST effect	76
5	SUMMARY	81
	LIST OF SYMBOLS	83
	BIBLIOGRAPHY	87
	PUBLICATIONS	95
	ACKNOWLEDGEMENT	97
	CURRICULUM VITAE	99
	EIDESSTÄTTLICHE ERKLÄRUNG	101

1 INTRODUCTION

Spintronics, which means “spin transport electronics” [1, 2] is a largely emerging technology since the 1980s. In contrast to electronics, which deals mainly with the transport of charge, this new technology adds the electrons spin as information carrier to practical devices [1]. The *spin*, a quantum mechanical property of elementary particles, is the intrinsic form of angular momentum. It was shown by STERN and GERLACH in 1922 that spin is in the presence of a quantization axis a quantized quantity and therefore only discrete spin quantum numbers are allowed [3]. Nowadays, the alignment of spins is used to store information. Namely, in presence of a quantization axis, which can be an external magnetic field or an internal magnetization, the spins align mainly parallel or antiparallel to this axis. These orientations are denoted as *spin up* and *spin down*, respectively. As a result, the spin is suitable as information carrier for example in the form of moving magnetic domains as used in the racetrack memory [4]. Two opposite orientations of the domains can be interpreted as 0 and 1. Consequently, data can be stored as binary numbers. A main aim to increase the variety of spintronic devices therefore is the generation, manipulation and detection of spin currents as well as the optimization of spin relaxation times and spin diffusion lengths, which allow information transport over sufficiently large length scales. One advantage of spintronic devices is the possibility to transport spin currents without effective charge flow, which should decrease the power consumption. In general, spintronic devices can be faster, more efficient and more reliable for long time storage applications than devices that are charge-based [1, 5].

The most prominent example with respect to this is the effect of giant magnetoresistance (GMR) [6, 7], whose observation was honoured with a Nobel prize in physics for Albert FERT and Peter GRÜNBERG in 2007 [8]. The GMR effect occurs in ferromagnet/non-magnet/ferromagnet multilayers, which have different resistivities for parallel and antiparallel orientation of the two magnetizations due to

spin-dependent scattering [6, 7]. Later, this effect was used by Stuart PARKIN to develop read-out heads, which were part of most hard disks since the late 90s [9]. Nowadays, the effect of tunnel magnetoresistance (TMR) is used in practical devices, where in comparison to the GMR effect the non-magnetic metal layer is replaced by an insulator [10].

In fact, at first all available spintronic devices just had the purpose to store or read information [5]. However, apart from that it became an essential task to generate especially pure spin currents to clear the way for a wider range of applications. A promising phenomenon in this regard is the spin HALL effect, which offers a way for a charge to spin current conversion. It is a bulk effect in metals and semiconductors including spin-orbit interaction. If a charge current is flowing through such a material, electrons are deflected in opposite directions depending on their spin orientation. This is caused by extrinsic and intrinsic mechanisms, which will be considered in Sec. 2.3. As a result, a transverse spin accumulation or spin current occurs, without any charge current in this direction. The beauty of this effect lies in the fact that it also works the other way around. Namely, via the inverse spin HALL effect a spin current can be transformed back into a charge current and therefore a perfect tool for the detection of spin currents is provided [11]. It was shown theoretically by GRADHAND et al. [12, 13, 14] that the sign and size of the spin HALL effect in dilute alloys is strongly dependent on the type of substitutional impurities. In the present work it is one focus point to investigate this effect in ternary alloys. The question is whether it is possible to enhance the efficiency of the charge to spin current conversion, if two different types of impurities are present (see Sec. 4.3 & 4.4.1).

Recently, the field *Spin caloritronics* [15, 16] gained importance, which couples the transport of charge, heat and spin. After a first pioneering work by JOHNSON and SILSBEE in 1987 [17] there was nearly no progress for about two decades. However, with the discovery of the spin SEEBECK effect by UCHIDA et al. [18] in 2008, this field experienced an uplift. The spin SEEBECK effect refers to the generation of a spin-motive force in a ferromagnetic strip by an applied temperature gradient. This leads to a detectable linearly varying transverse voltage in normal metal contacts via the inverse spin HALL effect [18]. Originally, the phenomenon was explained by a difference of the spin-dependent SEEBECK coefficients [19]. However, this explanation became unsustainable after the effect was also observed in magnetic insulators [20] and semiconductors [21]. Therefore, the phenomenon was finally considered as magnon-driven effect [22]. Although, the concept of spin-dependent

SEEBECK coefficients was not helpful to explain the spin SEEBECK effect, it is still useful to describe other phenomena, for instance a thermally driven spin injection from a ferromagnet to a nonmagnetic material [23]. In the present work this concept is applied to the spin NERNST effect, where a temperature gradient creates a transverse spin accumulation or spin current. After an introduction about general transport coefficients (Sec. 3.2.2) the necessary formula for the theoretical description of this effect are derived (Sec. 3.2.4). In the following, the physical properties, which quantify the created spin accumulation or spin current, are calculated for different types of impurities in a Cu host as functions of temperature (Sec. 4.1).

The systems are treated with a relativistic KORRINGA-KOHN-ROSTOKER method (Sec. 3.1.2), which is based on density functional theory (Sec. 3.1.1). It is worth to mention that in the presented study only the electronic contributions are considered while the influence of phonons is neglected. The dominating contribution to the spin HALL and spin NERNST effect in dilute alloys is provided by the skew-scattering mechanism, which causes asymmetric spin-dependent scattering at substitutional impurities in an otherwise ideal crystal. The skew-scattering mechanism is described in the BOLTZMANN approach via the microscopic transition probability in the scattering-in term. The electronic, thermal and spin transport properties can be extracted from the spin and energy dependent mean free path, which is obtained by solution of a linearized BOLTZMANN equation (Sec. 3.2.1). For some transport properties a numerical integration over an energy range around the FERMI level is necessary (Sec. 3.3.2). These methods are applied to systems consisting of a Cu host with one or two types of substitutional impurities, which are named binary and ternary alloys, respectively.

Apart from full calculations, where the scattering is treated by a superposition of the transition probabilities in the scattering term for the ternary alloys [24] (Sec. 3.3.1), it is possible to approximate their transport properties via MATTHIESSEN'S rule (Sec. 3.2.5). This rule assumes that non-interacting scattering processes can be treated independently from each other [25], which is considered by adding the corresponding resistivities to obtain the total resistivity. Then, MATTHIESSEN'S rule allows to estimate the transport properties of a ternary alloy simply from the properties of the constituent binary alloys. It seems reasonable that this assumption is a good approximation for dilute alloys, where the distance between the impurities is relatively large. It is tested whether this rule gives satisfying results. Of further interest is to analyse the nature of the deviations of the full calculation from MATTHIESSEN'S rule (Sec. 4.3).

However, the main aim of the investigations of the ternary alloys is to show, whether the spin HALL and spin NERNST effect can be enhanced with respect to the constituent binary alloys (Sec. 4.4). In fact, this is the case and therefore it opens a way to tune materials particularly for spintronics applications, where the efficiency of the spin current generation has to be optimized.

2 TRANSVERSE SPIN TRANSPORT PHENOMENA

2.1 CLASSIFICATION

The topic of this work is related to the spin HALL and spin NERNST effect, which are spin-dependent transport phenomena. They are classified in a family of HALL- and NERNST-type effects, as illustrated in Fig. 2.1. The source of these phenomena is either an applied electric field (HALL-type) or a temperature gradient (NERNST-type). All of them have in common that a transverse charge or spin accumulation or both are created.

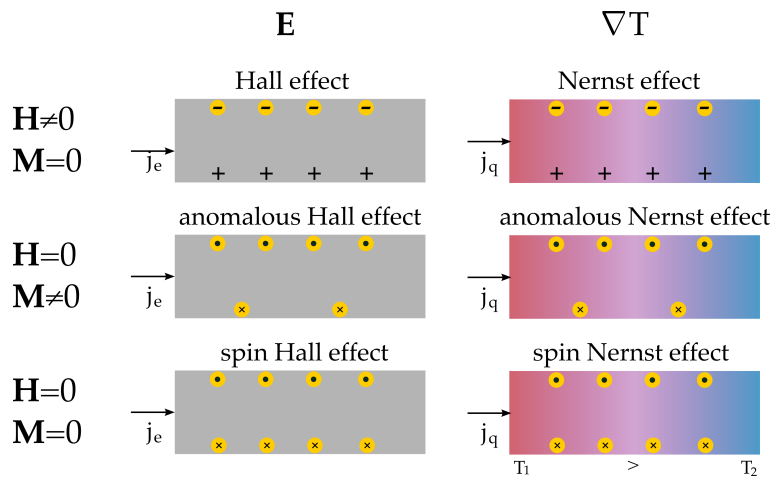


Figure 2.1: Classification of the HALL- & NERNST-type effects

The ordinary HALL and NERNST effect are well-known for a long time. An important condition for their observation is an external magnetic field perpendicular to

the electric field and temperature gradient, respectively. In both cases this results in a transverse charge accumulation, since moving charge carriers are deflected by the Lorentz force. The size of the effects is obtained by measuring an electrical voltage in direction of the charge accumulation.

The other four effects became very attractive just recently during the development of the fields *spintronics* [1, 2] and *spin caloritronics* [15, 16]. These phenomena are mainly caused by three mechanisms, which are explained in Sec. 2.3. The spin HALL (NERNST) effect has the same origin as the corresponding anomalous effect and therefore they can be discussed on an equal footing. An important point is that for an observation of these effects no external magnetic field is necessary. Instead, spin-orbit interaction has to be present. Then electrons with opposite spin orientations move in different directions and create a spin accumulation perpendicular to the spin direction and the applied electrical field or temperature gradient. The corresponding anomalous effects occur in magnetic materials, which means the number of spin-up and spin-down electrons is different. As a result, a charge accumulation in addition to the spin accumulation is present.

2.2 OBSERVATION

Whereas, no direct experimental confirmation of the spin NERNST effect is realized yet, the spin HALL EFFECT was already observed in 2004 by KATO et al. [26]. They used Kerr rotation as a method for an optical measurement of this phenomenon in GaAs. Figure 2.2 shows the obtained spin density in the plane, which is perpendicular to the polarization axis of the spins. Spin accumulations at the lateral edges of the sample were observed. It seems reasonable to apply this technique

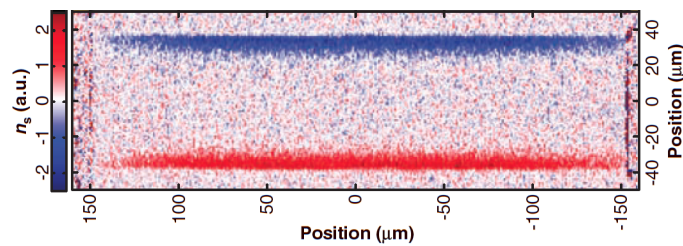


Figure 2.2: Two-dimensional image of the spin density n_s in GaAs [26].

also for a detection of the spin NERNST effect. However, materials, which provide strong spin accumulations, are required. It is part of this work to clarify which systems are suitable for an observation of this effect.

2.3 MECHANISMS

For the considered phenomena exist three main contributions, which are the intrinsic contribution and the extrinsic skew-scattering and side-jump mechanisms [27].

INTRINSIC CONTRIBUTION

The intrinsic contribution was first described by KARPLUS and LUTTNER in 1954 [28]. However, it took half a century until the topological nature of this effect [29, 30] including the relation between the BERRY phases and the anomalous velocity [31, 32] was understood. The contribution is called intrinsic, because it is caused by the intrinsic properties of a crystal and not by perturbations. Namely, it can be solely described in terms of the band structure of an ideal crystal. In detail, this contribution shows up as an additional term in the group velocity, which is given by [32]

$$v_k = \frac{1}{\hbar} \frac{\partial \mathcal{E}_k}{\partial k} + \underbrace{\frac{e}{\hbar} \mathbf{E} \times \boldsymbol{\Omega}_k}_{v_a} . \quad (2.1)$$

The anomalous velocity v_a is obviously perpendicular to the applied electric field \mathbf{E} and the so-called BERRY curvature $\boldsymbol{\Omega}_k$ and therefore provides a transverse current. The BERRY curvature arises via the concept of the BERRY phase. This theory states that if a HAMILTON operator of a quantum mechanical system runs through a closed path in its parameter space, then the corresponding wave function accumulates a geometric phase, the BERRY phase [33]. This phase as well as the BERRY curvature occur in systems with a complex HAMILTONIAN, for instance in the presence of spin-orbit coupling. As was shown by YAO et al. [34] especially avoided crossings in the band structure produce a high BERRY curvature of opposite sign for the upper and lower band. If the avoided crossing occurs exactly at the FERMI energy, then only one band is occupied. Therefore, this leads to a large contribution to the intrinsic spin HALL conductivity [35].

SKEW SCATTERING & SIDE JUMP

The skew-scattering and side-jump mechanism are extrinsic contributions, which means they are caused by scattering at impurities. The first description of the skew scattering was done by SMIT [36, 37]. This mechanism, which is visualized in Fig. 2.3, provides an asymmetric spin-dependent scattering. Due to its proportionality to the relaxation time, the skew-scattering mechanism is the dominant contribution in dilute alloys [27]. It is the reason, why only this mechanism is considered in this work. As will be discussed in Sec. 3.2.1, the skew scattering is well described within the traditional BOLTZMANN approach.

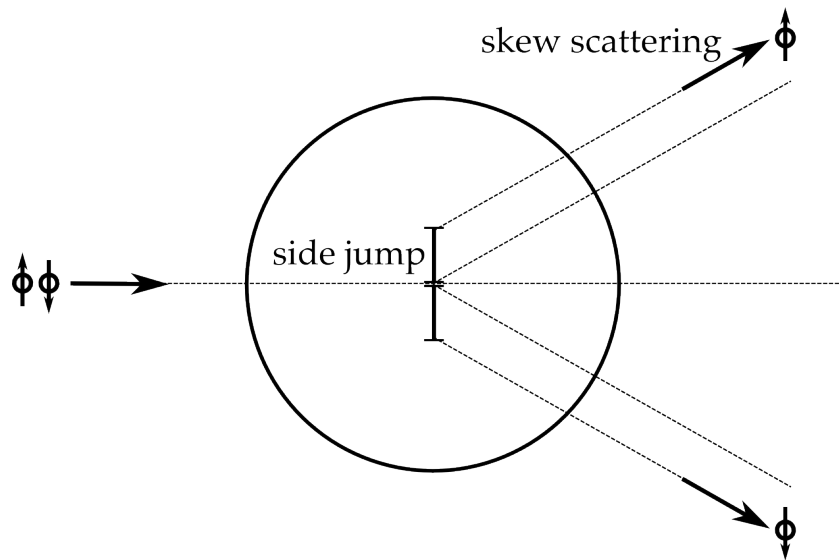


Figure 2.3: Illustration of the skew-scattering and side-jump mechanism.

The side jump is a phenomenon, which occurs in combination with the skew scattering due to the presence of impurities as shown in Fig. 2.3. However, the skew-scattering mechanism leads not to an instant change of the direction of the electron's motion. Instead, the electrons are smoothly deflected. Nevertheless, the asymptotic solutions of the incident and scattered electrons would meet exactly at the scattering center. In the presence of spin-orbit interaction the electrons leave the scattering potential a bit shifted in comparison to the path, which is

expected for the incident electrons when only skew scattering is present. This spin-dependent shift is known as side jump and was first described by BERGER [38, 39].

3 METHODS

3.1 ELECTRONIC STRUCTURE

3.1.1 DENSITY FUNCTIONAL THEORY

MANYBODY HAMILTONIAN & BORN-OPPENHEIMER APPROXIMATION

The main problem of solid state physics is the description of a many body system, which consists of interacting nuclei (c) and electrons (e). The corresponding HAMILTONIAN can be written as

$$H = T_e + T_c + V_{ee} + V_{ec} + V_{cc} , \quad (3.1)$$

where T and V are the kinetic energies and the interaction potentials of the indicated particles, respectively. It is too demanding to solve the corresponding SCHRÖDINGER equation

$$H |\Psi\rangle = \mathcal{E} |\Psi\rangle \quad (3.2)$$

exactly, since the system has degrees of freedom in the order of 10^{23} , namely the positions and momenta of each particle (electrons and nuclei). The first simplification for the solution of this problem is based on the BORN-OPPENHEIMER approximation [40], where the motion of the electrons is decoupled from the motion of the nuclei. This assumption is valid, since the COULOMB interaction between all particles is of the same order of magnitude. Due to their high mass in comparison to the electron mass the motion of the nuclei is negligible and therefore they are assumed to be static. Then the HAMILTONIAN for the electrons in an effective potential of the nuclei is given by:

$$H_e = T_e + V_{ee} + V_{ec} = \sum_{i=1}^{N_e} \frac{\vec{p}_i^2}{2m} + \sum_{i=1, i \neq j}^{N_e} \sum_{j=1}^{i-1} \frac{e^2}{|\vec{r}_i - \vec{r}_j|} + \sum_{i=1}^{N_e} V(\vec{r}_i) , \quad (3.3)$$

where T_e is the kinetic energy of the electrons, V_{ee} the interaction potential due to the COULOMB interaction between the electrons, and V_{ec} the interaction potential between electrons and nuclei.

THEOREMS OF HOHENBERG AND KOHN

A way to avoid the direct solution of the SCHRÖDINGER equation $H_e |\Psi_e\rangle = E |\Psi_e\rangle$, which still includes a term coupling the motion of all electrons via COULOMB interaction, is the density functional theory (DFT). This theory is based on the theorems of HOHENBERG and KOHN included in their work on the “Inhomogeneous Electron Gas” [41].

The essence of these theorems is:

In a system of interacting electrons with non-degenerate ground state the external potential is a functional of the ground state electron density apart from an additive constant [41].

Furthermore, for a given external potential exists an energy functional \mathcal{E} of the electronic density $n(\mathbf{r})$, which is minimal for the electronic density of the ground state $n_0(\mathbf{r})$ [41]

$$\mathcal{E}[n(\mathbf{r})] \equiv \int V(\mathbf{r})n(\mathbf{r})d\mathbf{r} + F[n(\mathbf{r})] , \quad (3.4)$$

$$\mathcal{E}_0 = E[n_0(\mathbf{r})] = \int V(\mathbf{r})n_0(\mathbf{r})d\mathbf{r} + F[n_0(\mathbf{r})] . \quad (3.5)$$

It is required to keep the condition

$$\int n(\mathbf{r})d\mathbf{r} = N_e , \quad (3.6)$$

which means the number of electrons N_e has to be conserved. Here, the density functionals of the kinetic energy and the interaction potential of the electrons are hidden in a functional $F[n(\mathbf{r})]$.

KOHN-SHAM EQUATIONS

A next step for the solution of the problem was proposed by KOHN and SHAM in 1965 [42]. Their main idea was to project the system of N_e electrons with interactions between each other to a system of non-interacting electrons in an effective one-particle potential. This was done by expressing the many particle wave function $|\Psi\rangle$ in terms of the single particle wave functions $|\psi_i\rangle$. Under this assumption,

the electronic density and the functional of the kinetic energy are simply described by

$$n(\mathbf{r}) = \sum_{i=1}^{N_e} |\psi_i(\mathbf{r})|^2 , \quad (3.7)$$

$$T_e[n(\mathbf{r})] = \sum_{i=1}^{N_e} \langle \psi_i | -\frac{\hbar^2}{2m} \nabla^2 | \psi_i \rangle . \quad (3.8)$$

The part of the electron-electron interaction in Eq. (3.3) is expressed by a contribution from the COULOMB interaction within the HARTREE approximation. Furthermore, it is necessary to introduce an additional functional $\mathcal{E}_{xc}[n(\mathbf{r})]$ to correct exchange and correlation effects. The energy functional then is given by

$$\mathcal{E}[n(\mathbf{r})] = T_e[n(\mathbf{r})] + \int V(\mathbf{r})n(\mathbf{r})d\mathbf{r} + \frac{e^2}{2} \iint \frac{n(\mathbf{r})n(\mathbf{r}')}{|\mathbf{r}-\mathbf{r}'|} d\mathbf{r}d\mathbf{r}' + \mathcal{E}_{xc}[n(\mathbf{r})] , \quad (3.9)$$

which has to be minimized to obtain the ground state. The minimization is performed via variation of $\mathcal{E}[n(\mathbf{r})]$ with respect to $|\psi_i\rangle$ under the condition of particle conservation

$$\delta\psi_i^* \left[\mathcal{E}[n(\mathbf{r})] - \sum_{i=1}^{N_e} \varepsilon_i \left(\int |\psi_i(\mathbf{r})|^2 d\mathbf{r} - 1 \right) \right] = 0 . \quad (3.10)$$

This leads to the following SCHRÖDINGER equation for the single particle wave functions with the effective potential $V_{eff}(\mathbf{r})$

$$\left[-\frac{\hbar^2}{2m} \nabla^2 + V_{eff}(\mathbf{r}) \right] \psi_i(\mathbf{r}) = \varepsilon_i \psi_i(\mathbf{r}) , \quad (3.11)$$

$$V_{eff}(\mathbf{r}) = V(\mathbf{r}) + \frac{e^2}{2} \int \frac{n(\mathbf{r}')}{|\mathbf{r}-\mathbf{r}'|} d\mathbf{r}' + \frac{\delta\mathcal{E}_{xc}[n(\mathbf{r})]}{\delta n(\mathbf{r})} . \quad (3.12)$$

These differential equations are known as KOHN-SHAM equations, where $\psi_i(\mathbf{r})$ and ε_i are in principle just auxiliary quantities, which allow the calculation of the electronic density and total energy of the system. The KOHN-SHAM equations can be solved iteratively. The iterative process, which can be schematically shown as

$$n(\mathbf{r}) \xrightarrow{\text{Eq. (3.12)}} V_{eff}(\mathbf{r}) \xrightarrow{\text{Eq. (3.11)}} \psi_i, \varepsilon_i \xrightarrow{\text{Eq. (3.7)}} n'(\mathbf{r}) , \quad (3.13)$$

←—————

is performed until the condition $n'(\mathbf{r}) = n(\mathbf{r})$ is fulfilled. One remaining problem is the correct form of the exchange-correlation potential. This is usually solved by further simplifications. For instance, the local density approximation (LDA)

$$\mathcal{E}_{xc}^{\text{LDA}}[n(\mathbf{r})] = \int d^3\mathbf{r} n(\mathbf{r}) \varepsilon_{xc}^{\text{hom}}[n(\mathbf{r})], \quad (3.14)$$

is widely used, which works well for slowly varying densities [42]. Here, the quantity $\varepsilon_{xc}^{\text{hom}}[n(\mathbf{r})]$ represents the exchange-correlation energy of one particle in a homogeneous, non-interacting electron gas.

3.1.2 KKR - A GREEN FUNCTION METHOD

The next step is the solution of the KOHN-SHAM equations to obtain the eigenvalues ε_i and eigenfunctions $\psi_i(\mathbf{r})$. For this aim the KORRINGA-KOHN-ROSTOKER (KKR) GREEN function method is used, which is based on the works of KORRINGA, KOHN, and ROSTOKER [43, 44]. An advantage is that the GREEN function contains all information about the electron properties of a considered system. Furthermore, this method offers the possibility to use the results from a known reference system to obtain the solution for an unknown one via the DYSON equation. Originally, the reference was related to free electrons. Within a screened KKR method as used in this work, the reference system corresponds to repulsive potentials of constant height centered at the atomic positions [45, 46, 47].

GREEN FUNCTION & PROPERTIES

The GREEN function G is the resolvent of the HAMILTON operator H defined via

$$(z\mathbb{1} - H)G(z) = \mathbb{1}, \quad (3.15)$$

where $\mathbb{1}$ is the unit operator. The complex energy variable $z = \mathcal{E} + i\eta$ is used, because the GREEN function has poles at the eigenenergies of H . Since only real energy values are of physical interest, it is required to determine the limit

$$\lim_{\eta \rightarrow \pm 0} = G^{\pm}(\mathcal{E}). \quad (3.16)$$

Here, $G^+(\mathcal{E})$ and $G^-(\mathcal{E})$ are known as retarded and advanced GREEN function, which describe outgoing and incoming waves, respectively. If a complete set of

eigenfunctions $|\psi_i\rangle$ of the HAMILTONIAN is known, a spectral representation of the GREEN function can be obtained in the following form

$$G^\pm(\mathcal{E}) = \lim_{\eta \rightarrow \pm 0} \sum_i \frac{|\psi_i\rangle \langle \psi_i|}{\mathcal{E} + i\eta - \varepsilon_i} \quad (3.17)$$

or in its position representation

$$G^\pm(\mathbf{r}, \mathbf{r}', \mathcal{E}) = \langle \mathbf{r} | G(\mathcal{E}) | \mathbf{r}' \rangle = \lim_{\eta \rightarrow \pm 0} \sum_i \frac{\psi_i(\mathbf{r}) \psi_i^*(\mathbf{r}')}{\mathcal{E} + i\eta - \varepsilon_i} . \quad (3.18)$$

By using the so-called DIRAC identity

$$\lim_{\eta \rightarrow \pm 0} \frac{1}{\mathcal{E} \pm i\eta - \varepsilon_i} = \mp i\pi \delta(\mathcal{E} - \varepsilon_i) + PV \left(\frac{1}{\mathcal{E} - \varepsilon_i} \right) \quad (3.19)$$

with the CAUCHY principal value PV one can express the difference between the retarded and advanced GREEN function by

$$G^+(\mathbf{r}, \mathbf{r}', \mathcal{E}) - G^-(\mathbf{r}, \mathbf{r}', \mathcal{E}) = -2i\pi \sum_i \psi_i(\mathbf{r}) \psi_i^*(\mathbf{r}') \delta(\mathcal{E} - \varepsilon_i) . \quad (3.20)$$

The local density of states of a system is defined via

$$n(\mathbf{r}, \mathcal{E}) = \sum_i \delta(\mathcal{E} - \varepsilon_i) |\psi_i(\mathbf{r})|^2 . \quad (3.21)$$

With Eq. (3.20) for $\mathbf{r} = \mathbf{r}'$ and the property

$$\Im \{ G^+(\mathcal{E}) \} = \frac{1}{2i} (G^+(\mathcal{E}) - G^-(\mathcal{E})) \quad (3.22)$$

for the imaginary part \Im of the retarded GREEN function follows

$$n(\mathbf{r}, \mathcal{E}) = \frac{i}{2\pi} (G^+(\mathbf{r}, \mathbf{r}, \mathcal{E}) - G^-(\mathbf{r}, \mathbf{r}, \mathcal{E})) = -\frac{1}{\pi} \Im \{ G^+(\mathbf{r}, \mathbf{r}, \mathcal{E}) \} . \quad (3.23)$$

From this quantity the density of states (DOS)

$$n(\mathcal{E}) = \int d^3\mathbf{r} n(\mathbf{r}, \mathcal{E}) = -\frac{1}{\pi} \Im \{ Tr \{ G^+(\mathcal{E}) \} \} \quad (3.24)$$

or the charge density

$$n(\mathbf{r}) = \int_{-\infty}^{\mathcal{E}_F} d\mathcal{E} n(\mathbf{r}, \mathcal{E}) = -\frac{1}{\pi} \int_{-\infty}^{\mathcal{E}_F} d\mathcal{E} \Im \{ G^+(\mathbf{r}, \mathbf{r}, \mathcal{E}) \} \quad (3.25)$$

can be obtained by taking the integral over the space and the energy, respectively.

DYSON & LIPPMANN-SCHWINGER EQUATION

The use of GREEN functions is an elegant option, which can be applied in scattering theory. Namely, it is possible to obtain the GREEN function $G(z)$ for a systems with HAMILTON operator $H = \mathring{H} + V$, if the GREEN function of a reference system corresponding to \mathring{H} is known. The two HAMILTONIANS then only differ by a scalar quantity (e.g. a scattering potential). From Eq. (3.15) the corresponding GREEN functions are the following

$$G(z) = (z\mathbb{1} - H)^{-1} , \quad \mathring{G}(z) = (z\mathbb{1} - \mathring{H})^{-1} . \quad (3.26)$$

They can be related to each other via the DYSON equation [48]

$$G(z) = \mathring{G}(z) + \mathring{G}(z)V G(z) = \mathring{G}(z) + G(z)V \mathring{G}(z) . \quad (3.27)$$

Repeated insertion of the DYSON equation in itself creates an iterative solution for $G(z)$. Using the so-called T operator, the GREEN function of the perturbed system can be written as

$$G(z) = \mathring{G}(z) + \mathring{G}(z)(V + V \mathring{G}(z)V + \dots)\mathring{G}(z) = \mathring{G}(z) + \mathring{G}(z)T(z)\mathring{G}(z) . \quad (3.28)$$

Similar to the DYSON equation there exists the LIPPMANN-SCHWINGER equation, which relates the perturbed and unperturbed wave functions via the corresponding GREEN functions, T operator and the potential V . If the wave functions are defined via the SCHRÖDINGER equations

$$H|\psi_i\rangle = (\mathring{H} + V)|\psi_i\rangle = \varepsilon_i|\psi_i\rangle , \quad \mathring{H}|\mathring{\psi}_i\rangle = \varepsilon_i|\mathring{\psi}_i\rangle , \quad (3.29)$$

then the LIPPMANN-SCHWINGER equation is given by [48]

$$|\psi_i\rangle = |\mathring{\psi}_i\rangle + \mathring{G}V|\psi_i\rangle = |\mathring{\psi}_i\rangle + GV|\mathring{\psi}_i\rangle = |\mathring{\psi}_i\rangle + \mathring{G}T|\mathring{\psi}_i\rangle . \quad (3.30)$$

with the T operator

$$T = V(\mathbb{1} - \mathring{G}V)^{-1} . \quad (3.31)$$

3.1.3 RELATIVISTIC KKR METHOD

A relativistic version of the KKR method [49, 50, 51, 52] is essential for the description of the considered phenomena. In the following the application of the density

functional theory to the DIRAC equation is shown. Furthermore, the muffin-tin and atomic sphere approximation are introduced, which offer a simplification of the scattering potential. As a result, the crystal is divided into cells, where the scattering at each site can be considered separately. Finally, the multiple scattering can be described under the assumption that an incoming wave at a scatterer is composed of the outgoing waves from all other sites [53]. These steps are done in the so-called $\kappa\mu$ -representation, where the relativistic quantum numbers are introduced.

DIRAC EQUATION

The aim of the present work is the investigation of spin-dependent transport phenomena caused by spin-orbit interaction. Therefore, a relativistic KKR method is used, where spin-orbit interaction is included. For this purpose the stationary DIRAC equation with the HAMILTON operator

$$H = c\hat{\alpha} \cdot \mathbf{p} + \hat{\beta}mc^2 + \hat{V}(\mathbf{r}) \quad (3.32)$$

is solved. Here, the matrices $\hat{\alpha}$ and $\hat{\beta}$ are expressed by the PAULI spin matrices $\hat{\sigma}_i$ and the 2×2 unit matrix $\mathbb{1}_2$:

$$\hat{\alpha}_i = \begin{pmatrix} 0 & \hat{\sigma}_i \\ \hat{\sigma}_i & 0 \end{pmatrix}, \quad \hat{\beta} = \begin{pmatrix} \mathbb{1}_2 & 0 \\ 0 & -\mathbb{1}_2 \end{pmatrix}. \quad (3.33)$$

The application of the density functional theory to the DIRAC equation leads to the KOHN-SHAM-DIRAC-HAMILTONIAN [54] with the potential in Eq. (3.32) given by

$$\hat{V}(\mathbf{r}) = V^{\text{eff}}[n(\mathbf{r}), \mathbf{m}(\mathbf{r})]\mathbb{1}_4 + \hat{\beta}\hat{\Sigma} \cdot \mathbf{B}^{\text{eff}}[n(\mathbf{r}), \mathbf{m}(\mathbf{r})], \quad \hat{\Sigma}_i = \begin{pmatrix} \hat{\sigma}_i & 0 \\ 0 & \hat{\sigma}_i \end{pmatrix}. \quad (3.34)$$

The effective scalar potential

$$V^{\text{eff}}[n(\mathbf{r}), \mathbf{m}(\mathbf{r})] = V(\mathbf{r}) + \int d^3\mathbf{r}' \frac{e^2 n(\mathbf{r})}{|\mathbf{r} - \mathbf{r}'|} + \frac{\delta \mathcal{E}_{xc}[n(\mathbf{r}), \mathbf{m}(\mathbf{r})]}{\delta n(\mathbf{r})} \quad (3.35)$$

is similar to the non-relativistic case for magnetic systems, where the exchange-correlation energy not only depends on the charge density n , but also on the magnetization density \mathbf{m} . The effective magnetic field is given by

$$\mathbf{B}^{\text{eff}}[n(\mathbf{r}), \mathbf{m}(\mathbf{r})] = \mathbf{B}(\mathbf{r}) + \frac{e\hbar}{2mc} \frac{\delta \mathcal{E}_{xc}[n(\mathbf{r}), \mathbf{m}(\mathbf{r})]}{\delta \mathbf{m}}, \quad (3.36)$$

where \mathbf{B} is an external magnetic field.

MUFFIN-TIN & ATOMIC SPHERE APPROXIMATION

Within the KKR method it is helpful to use spherical symmetric potentials, which are centered at each atomic position n . This is done by dividing the crystal into non-overlapping cells of maximal size with radius R_{MT}^n , which is known as muffin-tin (MT) approximation. Then it makes sense to introduce cell-centered coordinates

$$\mathbf{r} \rightarrow \mathbf{R}^n + \mathbf{r} , \quad (3.37)$$

where \mathbf{R}^n points to the center of the cell n and \mathbf{r} from the center to a point within this cell. The potential of a crystal with one atom per unit cell then is a superposition of the scattering potentials at each atomic site

$$V(\mathbf{r}) = \sum_n V^n(|\mathbf{r} - \mathbf{R}^n|) , \quad (3.38)$$

where all V^n are identical. To obtain the muffin-tin landscape of the potential one assumes that the potential is constant outside the muffin-tin radius while inside it has a spherically symmetric form

$$V^n(\mathbf{r} - \mathbf{R}^n) = \begin{cases} V_{\text{atom}}^n(|\mathbf{r} - \mathbf{R}^n|) & \text{if } |\mathbf{r} - \mathbf{R}^n| < R_{\text{MT}}^n \\ 0 & \text{otherwise} \end{cases} . \quad (3.39)$$

The problematic part of this approximation is the relatively large interstitial region with constant potential. Its possible extension is the so-called atomic sphere approximation (ASA), where the spheres are expanded up to the volume of the WIGNER-SEITZ cell. Of course, this leads to an overlap region, where the contributions are counted twice. However, they are partially compensated by the missing contributions from the remaining interstitial regions of equal size. Normally, this method works well, if the quantities are varying slowly. In particular, it gives good results for metals [54, 55].

SINGLE-SITE & MULTIPLE SCATTERING

The differential equation for the GREEN function of the SCHRÖDINGER equation is given by

$$\left[\mathcal{E} + \frac{\hbar^2}{2m} \frac{d^2}{dr^2} - V^n(r) \right] G(\mathbf{R}^n + \mathbf{r}, \mathbf{R}^{n'} + \mathbf{r}', \mathcal{E}) = \delta_{n,n'} \delta(\mathbf{r} - \mathbf{r}') , \quad (3.40)$$

which becomes homogeneous, if $\mathbf{R}^n \neq \mathbf{R}^{n'}$. It is a usual way to expand the GREEN function into the regular solutions of a single-site scatterer

$$R_L^n(\mathbf{r}, \mathcal{E}) = R_l^n(r, \mathcal{E})Y_L(\hat{\mathbf{r}}), \quad L = (l, m). \quad (3.41)$$

They include the spherical harmonics Y_L as well as the regular solutions of the radial SCHRÖDINGER equation with potential $V^n(r)$ [48]. The GREEN function is given by the following equation

$$G(\mathbf{R}^n + \mathbf{r}, \mathbf{R}^{n'} + \mathbf{r}', \mathcal{E}) = \delta_{mm'}G^n(\mathbf{R}^n + \mathbf{r}, \mathbf{R}^n + \mathbf{r}', \mathcal{E}) + \sum_{L, L'} R_L^n(\mathbf{r}, \mathcal{E})G_{LL'}^{nn'}(\mathcal{E})R_{L'}^{n'}(\mathbf{r}', \mathcal{E}), \quad (3.42)$$

where the second term describes the multiple-scattering processes between all muffin-tin potentials via the so-called structure constants $G_{LL'}^{nn'}(E)$. The first term includes the single-scattering solution $G^n(\mathbf{R}^n + \mathbf{r}, \mathbf{R}^n + \mathbf{r}', E)$ at an isolated muffin-tin potential in free space. It occurs due to the source term on the righthand side of Eq. (3.40).

$\kappa\mu$ -REPRESENTATION

As shown before, in the relativistic case the DIRAC HAMILTONIAN

$$H = c\hat{\boldsymbol{\alpha}} \cdot \mathbf{p} + \hat{\beta}mc^2 + V^{\text{eff}}(r)\mathbb{1}_4 + \hat{\beta}\hat{\boldsymbol{\Sigma}} \cdot \mathbf{B}^{\text{eff}}(r) \quad (3.43)$$

is used. Therefore, the resulting wavefunctions have the form of four-component spinors

$$\psi(\mathbf{r}) = \sum_Q c_Q R_Q(\mathbf{r}) = \sum_Q c_Q \sum_{Q'} \begin{pmatrix} g_{Q'Q}(r)\chi_{Q'}(\hat{\mathbf{r}}) \\ if_{Q'Q}(r)\chi_{\bar{Q}'}(\hat{\mathbf{r}}) \end{pmatrix}, \quad (3.44)$$

where $Q = \{\kappa, \mu_j\}$ and $\bar{Q} = \{-\kappa, \mu_j\}$ combine the relativistic quantum numbers

$$\kappa = \begin{cases} l = j + \frac{1}{2} & \text{if } j = l - \frac{1}{2} \\ -l - 1 = -(j + \frac{1}{2}) & \text{if } j = l + \frac{1}{2} \end{cases} \quad (3.45)$$

and

$$\mu_j \in \{-j, -j + 1, \dots, j - 1, j\}. \quad (3.46)$$

The quantities $\chi_Q(\hat{\mathbf{r}})$ are the spin spherical harmonics, which are defined via

$$\chi_Q(\hat{\mathbf{r}}) = \sum_{s=\pm\frac{1}{2}} C(l, \frac{1}{2}, j | \mu_j - s, s) Y_{l, \mu_j - s}(\hat{\mathbf{r}}) \Phi_s, \quad \Phi_{\frac{1}{2}} = \begin{pmatrix} 1 \\ 0 \end{pmatrix}, \quad \Phi_{-\frac{1}{2}} = \begin{pmatrix} 0 \\ 1 \end{pmatrix} \quad (3.47)$$

with the CLEBSCH-GORDON coefficients $C(l, \frac{1}{2}, j | \mu_j - s, s)$ and the spinor basis functions Φ_s [54]. If one applies the operators J^2 , J_z and $K = \boldsymbol{\sigma} \cdot \mathbf{L} + \mathbb{1}_2$ to the spin spherical harmonics

$$J^2 \chi_Q(\hat{\mathbf{r}}) = \hbar^2 j(j+1) \chi_Q(\hat{\mathbf{r}}), \quad (3.48)$$

$$J_z \chi_Q(\hat{\mathbf{r}}) = \hbar \mu_j \chi_Q(\hat{\mathbf{r}}), \quad (3.49)$$

$$K \chi_Q(\hat{\mathbf{r}}) = \hbar \kappa \chi_Q(\hat{\mathbf{r}}), \quad (3.50)$$

one obtains the quantum numbers of the total angular momentum j , its projection μ_j on the quantization axis, and of the relativistic angular momentum κ [54]. In the $\kappa\mu$ -representation the total GREEN function of Eq. (3.42) transforms to

$$G(\mathbf{R}^n + \mathbf{r}, \mathbf{R}^{n'} + \mathbf{r}', \mathcal{E}) = \delta_{nn'} G^n(\mathbf{R}^n + \mathbf{r}, \mathbf{R}^n + \mathbf{r}', \mathcal{E}) + \sum_{QQ'} R_Q^n(\mathbf{r}, \mathcal{E}) G_{QQ'}^{nn'}(E) R_{Q'}^{n'}(\mathbf{r}', \mathcal{E})^\times, \quad (3.51)$$

where the functions $R_Q(\mathbf{r})$ are defined by Eq. (3.44). For the corresponding functions

$$R_Q(\mathbf{r})^\times = \sum_{Q'} \left(g_{Q'Q}(\mathbf{r}) \chi_{Q'}(\hat{\mathbf{r}})^\dagger, -i f_{Q'Q}(\mathbf{r}) \chi_{\bar{Q}'}(\hat{\mathbf{r}})^\dagger \right) \quad (3.52)$$

only the conjugate complex of the non-radial part is taken [54]. The single-site GREEN function and the structure constants are connected to those of a reference system marked with \hat{G} by the DYSON equation

$$G^n(\mathbf{R}_n + \mathbf{r}, \mathbf{R}_n + \mathbf{r}', \mathcal{E}) = \hat{G}^n(\mathbf{R}_n + \mathbf{r}, \mathbf{R}_n + \mathbf{r}', \mathcal{E}) + \int d^3 \mathbf{r}'' \hat{G}^n(\mathbf{R}_n + \mathbf{r}, \mathbf{R}_n + \mathbf{r}'', \mathcal{E}) V^n(\mathbf{r}'') G^n(\mathbf{R}_n + \mathbf{r}'', \mathbf{R}_n + \mathbf{r}', \mathcal{E}), \quad (3.53)$$

$$G_{QQ'}^{nn'}(\mathcal{E}) = \hat{G}_{QQ'}^{nn'}(\mathcal{E}) + \sum_{Q'', Q''', n''} \hat{G}_{QQ''}^{nn''}(\mathcal{E}) t_{Q''}^{n''}(\mathcal{E}) G_{Q''Q'}^{n''n'}(\mathcal{E}). \quad (3.54)$$

Here, $V^n(r)$ is the difference between the potential of the physical and the reference system. The corresponding single-site t-matrix is given by [14]

$$\begin{aligned} t_{QQ'}^n(\mathcal{E}) &= \int d^3\mathbf{r} \hat{R}_Q^{n\times}(\mathbf{r}, \mathcal{E}) V^n(r) R_{Q'}^n(\mathbf{r}, \mathcal{E}) \\ &= \sum_{Q''} \int^{R_{ASA}^n} dr r^2 \left[\hat{g}_{Q''Q}^n(r) g_{Q''Q'}(r) + \hat{f}_{Q''Q}^n(r) f_{Q''Q'}(r) \right] V^n(r). \end{aligned} \quad (3.55)$$

For nonmagnetic systems as considered in this work the single-site t-matrix has a diagonal form $t_{QQ'}^n(\mathcal{E}) = \delta_{QQ'} t_Q^n(\mathcal{E})$ [56].

PERIODIC CRYSTALS

Periodic crystals have in each cell the same set of atoms and therefore the muffin-tin potential as well as the t-matrix do not depend on the cell index n . However, if the crystal has more than one atom per unit cell it is necessary to introduce an index μ for the basis atoms [47]. This leads to the following algebraic DYSON equation for the structure constants

$$G_{QQ'}^{\mu\mu'nm'}(\mathcal{E}) = \hat{G}_{QQ'}^{\mu\mu'nm'}(\mathcal{E}) + \sum_{Q'', n'', \mu''} \hat{G}_{QQ''}^{\mu\mu''nn''}(\mathcal{E}) t_{Q''}^{\mu''}(\mathcal{E}) G_{Q''Q'}^{\mu''\mu'nm'}(\mathcal{E}). \quad (3.56)$$

To solve this equation with the KKR method it is a usual way to use the FOURIER transform of the algebraic DYSON equation. The FOURIER transformed structure constants are given by

$$G_{QQ'}^{\mu\mu'}(\mathbf{k}, \mathcal{E}) = \sum_{n'} e^{i\mathbf{k}\mathbf{R}^{0n'}} G_{QQ'}^{\mu\mu'0n'}(\mathcal{E}), \quad (3.57)$$

which leads to an algebraic DYSON equation in k -space

$$G_{QQ'}^{\mu\mu'}(\mathbf{k}, \mathcal{E}) = \hat{G}_{QQ'}^{\mu\mu'}(\mathbf{k}, \mathcal{E}) + \sum_{Q'', \mu''} \hat{G}_{QQ''}^{\mu\mu''}(\mathbf{k}, \mathcal{E}) t_{Q''}^{\mu''}(\mathcal{E}) G_{Q''Q'}^{\mu''\mu'}(\mathbf{k}, \mathcal{E}). \quad (3.58)$$

It is possible to rewrite this equation into the following form

$$G_{QQ'}^{\mu\mu'}(\mathbf{k}, \mathcal{E}) = -\delta_{\mu\mu'} \delta_{QQ'} \left[t^{-1}(\mathcal{E}) \right]_Q^\mu - \left[t^{-1}(\mathcal{E}) \right]_Q^\mu \left[M^{-1}(\mathbf{k}, \mathcal{E}) \right]_{QQ'}^{\mu\mu'} \left[t^{-1}(\mathcal{E}) \right]_{Q'}^{\mu'} \quad (3.59)$$

with the so-called KKR-matrix

$$M_{QQ'}^{\mu\mu'}(\mathbf{k}, \mathcal{E}) = \hat{G}_{QQ'}^{\mu\mu'}(\mathbf{k}, \mathcal{E}) - \delta_{\mu\mu'} \delta_{QQ'} \left[t^{-1}(\mathcal{E}) \right]_Q^{\mu} . \quad (3.60)$$

Then the algebraic DYSON equation is solved by inversion of the KKR-matrix in combination with a FOURIER back transformation

$$G_{QQ'}^{\mu\mu'nn'}(\mathcal{E}) = \frac{1}{V_{\text{BZ}}} \int_{V_{\text{BZ}}} d^3\mathbf{k} e^{-i\mathbf{k}R^{nn'}} G_{QQ'}^{\mu\mu'}(\mathbf{k}, \mathcal{E}) . \quad (3.61)$$

REFERENCE SYSTEMS - SCREENED KKR AND IMPURITY PROBLEM

In the present work transport properties in the diffusive regime are investigated. For this reason metallic host systems with substitutional impurities are considered, whose GREEN functions are calculated with help of the algebraic DYSON equation. Actually, the results for the defect systems are reached via the following steps:

1. SCREENED REFERENCE SYSTEM

At first the structure constants for a screened reference system are calculated from the analytically known structure constants of free space as initial reference [45, 46, 47, 57]. The corresponding periodic potential of the screened system is repulsive at each atomic position and provides no unwanted eigenstates in the energy range, which is needed for self-consistent electronic structure calculations. The detour via the screened system is quite advantageous. Namely, it is known that the structure constants of the free space decay quite slowly with the distance between the atomic positions. Therefore, it is computationally demanding to calculate the FOURIER transform of those. In contrast, the structure constants of the screened reference system decay quite fast. Due to the short-range interaction they can be obtained by solving the algebraic DYSON equation in real space on a cluster of finite size.

2. HOST SYSTEM

A real periodic crystal has extended states which makes it now necessary to solve the algebraic DYSON equation in reciprocal space (Eq. (3.58)). There the difference of t-matrices for the host system and the screened reference system has to be used. Before, the FOURIER transformation is applied to the screened structure constants. However, this can be done quite easily, since the sum in

Eq. (3.57) runs over a finite number of atomic sites in the chosen cluster mentioned above. Furthermore, the short-range screened structure constants in real space can provide many vanishing components for the FOURIER transformed ones for special geometries, which can decrease the computational effort.

3. DEFECT SYSTEM

In this work, dilute alloys are considered, where the interactions between the impurities are negligible. Therefore, it is sufficient to treat only a single defect, while the total number of impurities is taken into account via their concentration. Since in metals perturbations are effectively screened [58], only a cluster with a few nearest-neighbour shells around the impurity have to be taken into account allowing a sufficient charge relaxation. For such an impurity cluster, the algebraic DYSON equation in real space can be solved, where the structure constants for the host atoms involved in the cluster are used. This provides the GREEN function of the defect system.

WAVE FUNCTIONS OF THE IDEAL CRYSTAL AND THE DEFECT SYSTEM

The wave functions of the ideal crystal are BLOCH functions, which are expanded in the single-site solutions

$$\psi_{\mathbf{k}}^{n\mu}(\mathbf{r}) = \frac{1}{\sqrt{V}} \sum_{\mathbf{Q}} e^{i\mathbf{k}\mathbf{R}^n} \hat{c}_{\mathbf{Q}}^{n\mu}(\mathbf{k}) \hat{R}_{\mathbf{Q}}^{n\mu}(\mathbf{r}), \quad (3.62)$$

and these wave functions are normalized. The determination of the expansion coefficients can be performed according to the Ph.D. thesis of P. ZAHN [46] for the non-relativistic case and to the Ph.D. thesis of M. GRADHAND [14] for the relativistic case. Similar to Eq. (3.62), the wave functions of the defect system have the form

$$\psi_{\mathbf{k}}^{n\mu}(\mathbf{r}) = \frac{1}{\sqrt{V}} \sum_{\mathbf{Q}} e^{i\mathbf{k}\mathbf{R}^n} c_{\mathbf{Q}}^{n\mu}(\mathbf{k}) R_{\mathbf{Q}}^{n\mu}(\mathbf{r}). \quad (3.63)$$

If this ansatz is used, the corresponding LIPPMANN-SCHWINGER equation can be transformed in an equation for the expansion coefficients only [59]

$$c_{\mathbf{Q}}^{n\mu}(\mathbf{k}) = \hat{c}_{\mathbf{Q}}^{n\mu}(\mathbf{k}) + \sum_{\mathbf{Q}'n'\mu'} \hat{G}_{\mathbf{Q}\mathbf{Q}'}^{nn'\mu\mu'}(\mathcal{E}) t_{\mathbf{Q}'}^{n'\mu'}(\mathcal{E}) c_{\mathbf{Q}'}^{n'\mu'}(\mathbf{k}). \quad (3.64)$$

Then, it is possible to obtain the coefficients of the perturbed system by the ones of the ideal crystal

$$c_Q^{n\mu}(\mathbf{k}) = \sum_{Q'n'\mu'} D_{QQ'}^{nn'\mu\mu'}(\mathcal{E}) c_{Q'}^{n'\mu'}(\mathbf{k}) \quad (3.65)$$

via the defect-matrix

$$D_{QQ'}^{nn'\mu\mu'}(\mathcal{E}) = \delta_{QQ'} \delta_{nn'} \delta_{\mu\mu'} + G_{QQ'}^{nn'\mu\mu'}(\mathcal{E}) t_{Q'}^{n'\mu'}(\mathcal{E}) = \left[\left(1 - \mathring{G}(\mathcal{E}) t(\mathcal{E}) \right)^{-1} \right]_{QQ'}^{nn'\mu\mu'}. \quad (3.66)$$

Here, the algebraic DYSON equation in Eq. (3.56) was used to express this quantity in terms of the perturbed GREEN function G .

BAND STRUCTURE, FERMI SURFACE & FERMI VELOCITY

One part of the work performed using the KKR method is the determination of the band structure, the FERMI surface and FERMI velocity. These features are presented here in a summarized way, while a detailed consideration can be found in the Ph.D. theses of Jörg BINDER [47], Peter ZAHN [46] and Martin GRADHAND [14].

The BLOCH functions of an ideal crystal are the solutions of the equation

$$(\mathcal{E} - \mathring{H}) \mathring{\psi}_k^{n\nu}(\mathbf{r}) = \mathring{G}^{-1}(\mathbf{r}, \mathbf{r}', \mathcal{E}) \mathring{\psi}_k^{n\nu}(\mathbf{r}) = 0. \quad (3.67)$$

With help of the DYSON equation

$$\mathring{G}(\mathcal{E}) = \tilde{G}(\mathcal{E}) + \tilde{G}(\mathcal{E}) (\mathring{V} - \tilde{V}) \mathring{G}(\mathcal{E}), \quad (3.68)$$

which relates the GREEN function of the ideal crystal \mathring{G} with the one of the screened reference system \tilde{G} , the BLOCH function is obtained via the following integral equation

$$\mathring{\psi}_k^{n\mu}(\mathbf{r}) = \sum_{n', \mu'} \int d^3 \mathbf{r}' \tilde{G}^{nn'\mu\mu'}(\mathbf{r}, \mathbf{r}', \mathcal{E}) (\mathring{V}(\mathbf{r}') - \tilde{V}(\mathbf{r}')) \mathring{\psi}_k^{n'\mu'}(\mathbf{r}). \quad (3.69)$$

Here, $\tilde{V}(\mathbf{r})$ is the repulsive potential of the screened reference system. The structure of this equation differs from the LIPPMANN-SCHWINGER equation, since due to the BLOCH theorem the incident waves are missing. The BLOCH ansatz for the unperturbed wave functions in Eq. (3.62) leads to an algebraic eigenvalue equation

$$\sum_{\mu'} \sum_{Q'} \left[\left[t^{-1}(\mathcal{E}) \right]_Q^{\mu} \delta_{\mu\mu'} \delta_{QQ'} - \tilde{G}_{QQ'}^{\mu\mu'}(\mathbf{k}, \mathcal{E}) \right] t_{Q'}^{\mu'}(\mathcal{E}) c_{Q'}^{\mu'}(\mathbf{k}) = 0, \quad (3.70)$$

from which the expansion coefficients $\hat{c}_{Q'}^{\mu'}(\mathbf{k})$ can be determined. With the definition of the KKR matrix in Eq. (3.60) used with the screened system as reference the above equation can be written as

$$\sum_{\mu'} \sum_{Q'} M_{QQ'}^{\mu\mu'}(\mathbf{k}, \mathcal{E}) t_{Q'}^{\mu'}(\mathcal{E}) \hat{c}_{Q'}^{\mu'}(\mathbf{k}) = 0. \quad (3.71)$$

The calculation of the band structure is performed by finding the vanishing eigenvalues of the KKR matrix $M(\mathbf{k}, \mathcal{E})$, which provides the dispersion relation $\mathcal{E}(\mathbf{k})$.

Since the KKR matrix is not hermitian, it is necessary to use transformations, which were explained by P. ZAHN [46] and M. GRADHAND [14]. The obtained eigenvalue equation is solved by using nested intervals for the energies.

For the calculation of the isoenergetic surfaces especially at the FERMI energy a tetrahedron method is used, where the reciprocal space of an irreducible part of the BRIOULLIN zone is completely filled with tetrahedra. Each tetrahedron is labeled and the corresponding corners and edges are assigned. Then on each edge is tested if one point of this line belongs to the FERMI energy. These resulting intersections of the tetrahedra provide the vertices of planes of triangular or quadrangular shape [46]. The planes, which are determined this way, form all together the FERMI surface of the system.

An important quantity, which enters into the transport calculations via the BOLTZMANN approach is the FERMI velocity. This is the group velocity on the FERMI surface and is given by

$$v_k^F = \left. \frac{1}{\hbar} \frac{\partial \mathcal{E}_k}{\partial \mathbf{k}} \right|_{\mathcal{E}=\mathcal{E}_F}. \quad (3.72)$$

To evaluate the \mathbf{k} derivative of the energy there exist two possible methods - a numerical one and another method, where it is obtained via the analytic \mathbf{k} derivative of the structure constants [14]. The analytic method is only necessary, if the FERMI surface has high curvatures, and is explained in Ref. [14]. However, since in the present work only a Cu host is considered, whose FERMI surface has an almost spherical shape, the numerical method is sufficient. For this purpose two additional isoenergetic surfaces are calculated, which belong to energies slightly above and below the FERMI energy and have an energy difference of $\Delta\mathcal{E}$. The FERMI velocity can be approximated by solving the following system of linear equations

$$\hbar(\Delta k_i) v_k^F = \Delta\mathcal{E}, \quad (3.73)$$

where Δk_i is the difference of the corresponding k points on edge i of a tetrahedron [46].

SPIN EXPECTATION VALUE

Due to the structure of the DIRAC-HAMILTONIAN the vector spin operator is given by [60]

$$\hat{\beta}\hat{\Sigma} = \begin{pmatrix} \mathbb{1}_2 & 0 \\ 0 & -\mathbb{1}_2 \end{pmatrix} \begin{pmatrix} \hat{\sigma} & 0 \\ 0 & \hat{\sigma} \end{pmatrix} = \begin{pmatrix} \hat{\sigma} & 0 \\ 0 & -\hat{\sigma} \end{pmatrix}, \quad (3.74)$$

which describes the interaction of the spins with an effective magnetic field in the DIRAC HAMILTONIAN of Eq. (3.43). The expectation value for the spin direction at each k point on the FERMI surface is obtained by

$$\mathbf{s}_k = \langle \hat{\psi}_k^{n\mu} | \hat{\beta}\hat{\Sigma} | \hat{\psi}_k^{n\mu} \rangle. \quad (3.75)$$

The investigated Cu host is a non-magnetic system with space inversion symmetry. Together with the present time-reversal symmetry, providing the KRAMERS degeneracy [61], this creates two degenerate states at each k point even when spin-orbit interaction is included [62, 63]. As a result, two orthonormal wave functions $\psi_k^{n\mu 1}$ and $\psi_k^{n\mu 2}$ exist at the same energy, but with opposite spin directions [64]

$$\langle \hat{\psi}_k^{n\mu 1} | \hat{\beta}\hat{\Sigma} | \hat{\psi}_k^{n\mu 1} \rangle = -\langle \hat{\psi}_k^{n\mu 2} | \hat{\beta}\hat{\Sigma} | \hat{\psi}_k^{n\mu 2} \rangle. \quad (3.76)$$

Since in the relativistic case the spin is not anymore a good quantum number, the wave functions can not simply be labeled by the spin states. Instead the wave functions are given by “any orthonormalized linear combinations of the two corresponding eigenfunctions” [63]. Two appropriate choices for such superpositions are discussed in the work of PIENKA et al. [63]. Each of them corresponds to a certain gauge. In the present work the second of them is used, where “one component of the spin operator is diagonalized with respect to the two degenerate states” [63]. However, in the mentioned paper is shown that both gauges lead to the same results for the calculation of the relaxation time for a Cu host material. After the gauge transformation with correct normalization and orthogonality of the wave functions is performed, the obtained wave functions can be labeled with (+) and (−), where the spin expectation value in z direction

$$s_k^{z+} = \langle \hat{\psi}_k^{n\mu+} | \hat{\beta}\hat{\Sigma}_z | \hat{\psi}_k^{n\mu+} \rangle = -\langle \hat{\psi}_k^{n\mu-} | \hat{\beta}\hat{\Sigma}_z | \hat{\psi}_k^{n\mu-} \rangle = -s_k^{z-} \quad (3.77)$$

is positiv and negativ, respectively.

TRANSITION MATRIX

An important quantity for the treatment of the scattering processes is the so-called transition matrix. It contains the BLOCH wave $\hat{\psi}$, the scattering potential V , and the perturbed wave ψ and is given by [65]

$$T_{kk'}^{vv'} = \frac{1}{V} \sum_{n\mu} \int d^3\mathbf{r} \left(\hat{\psi}_{k'}^{n\mu v'}(\mathbf{r}) \right)^\dagger V(r) \psi_k^{n\mu v}(\mathbf{r}) . \quad (3.78)$$

Here, the indices ν and ν' stand for the spin direction before and after the scattering process, respectively. If the BLOCH ansatz in Eqs. (3.62) and (3.63) with the expansion in single-site solutions is used in addition to Eq. (3.65), the transition matrix can be rewritten as

$$T_{kk'}^{vv'} = \frac{1}{V} \sum_{Q,n,\mu} \sum_{Q',n',\mu'} \left(\hat{c}^{n\mu v'}(\mathbf{k}') \right)^* \Delta_Q^{n\mu} D_{QQ'}^{nn'\mu\mu'}(\mathcal{E}) \hat{c}_{Q'}^{n'\mu'v}(\mathbf{k}) , \quad (3.79)$$

where the matrix $\Delta_Q^{n\mu}$ is given by the following radial integral

$$\Delta_Q^{n\mu} = \sum_{Q'} \int_0^{R_{\text{ASA}}^{n\mu}} dr r^2 \left(\left(\hat{g}_{QQ'}^{n\mu}(r) \right)^* g_{QQ'}^{n\mu}(r) + \left(\hat{f}_{QQ'}^{n\mu}(r) \right)^* f_{QQ'}^{n\mu}(r) \right) V(r) . \quad (3.80)$$

With the transition matrix it is possible to describe two types of scattering. Namely, the quantities $T_{kk'}^{++}$ and $T_{kk'}^{--}$ describe the spin-conserving scattering processes. The other two quantities ($T_{kk'}^{+-}$ and $T_{kk'}^{-+}$) refer to the spin-flip scattering, which means during the scattering process the electron changes not only its k vector, but also its spin direction. The spin-flip is caused by the ELLIOTT-YAFET mechanism [62, 66] occurring due to perturbations in an ideal crystal, which here are substitutional impurities. Depending on the type of scattering two different relaxation times τ_k and τ_k^{sf} are defined, which are the average times an electron in the state k can move before it is scattered without and with spin-flip, respectively. Usually, the spin-flip scattering time is long in comparison to the momentum relaxation time and therefore has only a small influence on the considered effects.

To simplify the equations later in this work a combined index $k = \{\mathbf{k}, \nu\}$ is used, where the state is not only characterized by the wave vector, but also by the band index ν . This leads to the transition matrix $T_{kk'}^{vv'} \rightarrow T_{kk'}$.

3.2 ELECTRONIC TRANSPORT

3.2.1 BOLTZMANN APPROACH

The use of the BOLTZMANN equation is a semiclassical approach for the investigation of electronic transport in solids. It can describe the influence of external fields or temperature gradients on statistical distributed particles in a medium. Originally, it was developed for the description of dilute gases. Here, the method is applied to dilute alloys, where electrons undergo the scattering at impurities.

The key quantity of the BOLTZMANN approach is the distribution function $f_k(\mathbf{r}, t)$, which describes the probability that a particle is in a state k at a place \mathbf{r} at a time t . The BOLTZMANN equation

$$\frac{\partial f_k(\mathbf{r}, t)}{\partial t} + \dot{\mathbf{r}}_k \frac{\partial f_k(\mathbf{r}, t)}{\partial \mathbf{r}} + \dot{\mathbf{k}} \frac{\partial f_k(\mathbf{r}, t)}{\partial \mathbf{k}} = \left[\frac{\partial f_k(\mathbf{r}, t)}{\partial t} \right]_{scatt.} \quad (3.81)$$

is given by the total time derivative of the distribution function on the left-hand side of the equation and a term considering scattering processes on the right-hand side. In this transport equation $\dot{\mathbf{r}}_k \equiv \mathbf{v}_k = \frac{1}{\hbar} \frac{\partial \mathcal{E}_k}{\partial \mathbf{k}}$ is the group velocity and $\dot{\mathbf{k}} = -\frac{e}{\hbar} (\mathbf{E} + \mathbf{v}_k \times \mathbf{B})$ provides the contribution of an external electric or magnetic field via the Lorentz force.

It is useful to represent the distribution function by a sum of the equilibrium part, given by the FERMI function

$$f_k^0(\mathbf{r}) = \left[e^{\frac{\mathcal{E}_k - \mu(\mathbf{r})}{k_B T(\mathbf{r})}} + 1 \right]^{-1}, \quad (3.82)$$

and a perturbed part g :

$$f_k(\mathbf{r}, t) = f_k^0(\mathbf{r}) + g_k(\mathbf{r}, t). \quad (3.83)$$

SCATTERING TERM

The scattering term in the BOLTZMANN equation is given by the perturbed part of the distribution function [67, 68]

$$\left[\frac{\partial f_k(\mathbf{r}, t)}{\partial t} \right]_{scatt.} = \left[\frac{\partial g_k(\mathbf{r}, t)}{\partial t} \right]_{scatt.} = \sum_{k'} (P_{k'k} g_{k'} - P_{kk'} g_k), \quad (3.84)$$

since in equilibrium scattering should give no contribution. Here, $P_{kk'}$ is the microscopic transition probability

$$P_{kk'} = \frac{2\pi}{\hbar} c_i N |T_{kk'}|^2 \delta(\mathcal{E}_k - \mathcal{E}_{k'}) \quad (3.85)$$

according to FERMI's golden rule, which is the probability that a particle from state k is scattered elastically into the state k' . Here, N and c_i denote the total number of atoms and the impurity concentration, respectively. The quantities $T_{kk'}$ are the elements of the transition matrix in Eq. (3.78).

For the description of the skew scattering it is important, that the conventional principle of the microscopic reversibility is not anymore valid in the relativistic case, were spin-orbit interaction is present. This means $P_{kk'} \neq P_{k'k}$ [12].

SOLUTION OF THE BOLTZMANN EQUATION

The quantities, which are investigated in this work are charge and spin accumulations as well as charge, spin, and heat currents obtained in linear response to an applied electric field or temperature gradient. The linearized form of the BOLTZMANN equation (3.81) is given by [69]

$$\left(-\frac{\partial f_k^0(\mathbf{r})}{\partial \mathcal{E}_k} \right) v_k \underbrace{\left[\frac{\mathcal{E}_k - \mu}{T} \nabla T + \nabla \mu + eE \right]}_{\mathbf{K}_k} = \sum_{k'} (P_{k'k} g_{k'} - P_{kk'} g_k) . \quad (3.86)$$

The nonequilibrium part of the distribution function can be written as

$$g_k = \frac{\partial f_k^0}{\partial \mathcal{E}_k} \boldsymbol{\Lambda}_k \cdot \mathbf{K}_k \quad (3.87)$$

in linear response to a generalized force \mathbf{K}_k , which is introduced to combine the influence of external electric fields, temperature gradients and gradients of the chemical potential. The quantity $\boldsymbol{\Lambda}_k$ is the vector mean free path, which has to be calculated. From the Eqs. (3.86) and (3.87) follows

$$\left(-\frac{\partial f_k^0}{\partial \mathcal{E}_k} \right) v_k \mathbf{K}_k = -\frac{1}{\tau_k} \frac{\partial f_k^0}{\partial \mathcal{E}_k} \boldsymbol{\Lambda}_k \cdot \mathbf{K}_k + \sum_{k'} \left(P_{k'k} \frac{\partial f_{k'}^0}{\partial \mathcal{E}_{k'}} \boldsymbol{\Lambda}_{k'} \cdot \mathbf{K}_{k'} \right) , \quad (3.88)$$

where the definition for the relaxation time $\tau_k = [\sum_{k'} P_{k'k}]^{-1}$ was used. Under the assumption of elastic scattering, which is included in $P_{k'k}$ given by Eq. (3.85), the equation above can be reduced to one for the mean free path

$$\Lambda_k = \tau_k \left[v_k + \sum_{k'} P_{k'k} \Lambda_{k'} \right]. \quad (3.89)$$

This equation is usually solved iteratively using $\Lambda_k^0 = \tau_k v_k$ as initial value [59]. With a corresponding final solution and Eq. (3.87) the charge and heat current density can be obtained as [69]

$$\mathbf{j} = -e \sum_k v_k g_k, \quad (3.90)$$

$$\mathbf{q} = \sum_k (\mathcal{E}_k - \mu) v_k g_k. \quad (3.91)$$

The sum over the combined index k contains sums over the bands as well as an integral over the reciprocal space. This can be split into an integral over the energy and an integral over isoenergetic surfaces in k space according to [47]

$$\sum_k \dots \rightarrow \sum_{\nu} \frac{1}{(2\pi)^3} \int d^3\vec{k} \dots = \frac{1}{8\pi^3} \sum_{\nu} \int d\mathcal{E} \iint_{\mathcal{E}_k=\mathcal{E}} \frac{dS_k}{\hbar|v_k|} \dots \quad (3.92)$$

3.2.2 TRANSPORT PROPERTIES

GENERAL TRANSPORT COEFFICIENTS

Using the definitions of the charge and heat current density above together with the Eqs. (3.87) and (3.92), relations between the current densities and the external or internal fields can be obtained as

$$\mathbf{j} = -e\hat{L}_0 \left(\mathbf{E} + \frac{1}{e} \nabla \mu \right) + \frac{1}{T} \hat{L}_1 (-\nabla T), \quad (3.93)$$

$$\mathbf{q} = \hat{L}_1 \left(\mathbf{E} + \frac{1}{e} \nabla \mu \right) - \frac{1}{eT} \hat{L}_2 (-\nabla T). \quad (3.94)$$

The relations are described by the general transport coefficients

$$\hat{L}_n(T) = -\frac{1}{e} \int \hat{\sigma}(\mathcal{E}) \left(-\frac{\partial f^0(\mathcal{E}, T)}{\partial \mathcal{E}} \right) (\mathcal{E} - \mu)^n d\mathcal{E}, \quad n = 0, 1, 2. \quad (3.95)$$

These coefficients are temperature dependent via the derivative of the FERMI function. The integral in Eq. (3.95) contains the energy-dependent conductivity tensor

$$\hat{\sigma}(\mathcal{E}) = \frac{e^2}{\hbar(2\pi)^3} \sum_{\nu} \iint_{\mathcal{E}_k=\mathcal{E}} \frac{dS_k}{|\mathbf{v}_k|} \mathbf{v}_k \circ \mathbf{\Lambda}_k . \quad (3.96)$$

In practice, only a small energy range around the FERMI level is necessary for a sufficiently correct integration in Eq. (3.95), since the derivative of the FERMI function is strongly decaying with distance from the FERMI energy.

With the knowledge of the general transport coefficients several transport properties can be described.

CHARGE CONDUCTIVITY

In linear response, the charge conductivity tensor $\hat{\sigma}$ is defined via OHM's law

$$\mathbf{j} = \hat{\sigma} \mathbf{E} \quad (3.97)$$

and in terms of the transport coefficients is given by $\hat{\sigma}(T) = -e\hat{L}_0(T)$. Therefore, the electronic contribution to the conductivity is in principle temperature dependent. However, due to the nearly linear behaviour of $\hat{\sigma}(\mathcal{E})$ around the FERMI level obtained for the considered systems, the quantity $\hat{L}_0(T)$ is approximately constant. Consequently, the conductivity can be obtained as

$$\hat{\sigma} = -e\hat{L}_0(T=0) = \hat{\sigma}(\mathcal{E}_F) , \quad (3.98)$$

according to the discussion in Sec. 4.1.1.

SPIN CONDUCTIVITY

The used nomenclature also allows the description of spin-dependent transport phenomena. Let us assume that there is only one conduction band at the FERMI energy, as in the case of copper, then the index ν corresponds to the two degenerate relativistic spin states $\nu = +$ (spin-up) and $\nu = -$ (spin-down) [64, 12]. Consequently, the conductivity can be expressed for each spin direction separately

$$\hat{\sigma}^{\nu}(\mathcal{E}) = \frac{e^2}{\hbar(2\pi)^3} \iint_{\mathcal{E}_k=\mathcal{E}} \frac{dS_k}{|\mathbf{v}_k|} \mathbf{v}_k \circ \mathbf{\Lambda}_k , \quad \nu = +, - , \quad (3.99)$$

which leads to spin-dependent general transport coefficients $\hat{L}_n^v(T)$. Furthermore, the conductivity can be represented in a two-current description as $\hat{\sigma} = \hat{\sigma}^+ + \hat{\sigma}^-$, where it is assumed that the two spin channels behave as resistors in a parallel circuit.

An important quantity for the description of the spin HALL effect is the spin HALL conductivity, which is an off-diagonal element of the spin conductivity tensor [12]

$$\hat{\sigma}^s(\mathcal{E}) = \frac{e^2}{\hbar(2\pi)^3} \sum_v \iint_{\mathcal{E}_k=\mathcal{E}} \frac{dS_k}{|v_k|} s_k^z v_k \circ \mathbf{\Lambda}_k . \quad (3.100)$$

This quantity is similar to $\hat{\sigma}(\mathcal{E})$, but includes the spin expectation value in z direction. In general, this quantity has two further components referring to the x and y direction, since the spin polarization \mathbf{s}_k is a vector quantity. However, in the following the gauge is chosen to align the spins along the z direction and therefore only the spin conductivity in the above presented form is of interest. In the non-relativistic description, where spin-orbit interaction is excluded, the two current model holds for the spin conductivity as

$$\hat{\sigma}^s = \hat{\sigma}^+ - \hat{\sigma}^- , \quad (3.101)$$

since the spin expectation value has the opposite sign for the two spin directions and an absolute value of one.

HEAT CONDUCTIVITY

The heat conductivity $\hat{\kappa}$ relates the heat current density to the temperature gradient

$$\mathbf{q} = \hat{\kappa} (-\nabla T) . \quad (3.102)$$

The heat current in response to an external temperature gradient is usually measured with an open circuit condition, where no charge current is flowing ($\mathbf{j} = 0$). Due to Eq. (3.93) this leads to a charge accumulation given by

$$\nabla \mu = \frac{1}{T} \hat{L}_0^{-1} \hat{L}_1 (-\nabla T) . \quad (3.103)$$

Substituting it in Eq. (3.94), the heat conductivity is obtained as

$$\hat{\kappa} = \frac{1}{eT} \left(\hat{L}_1 \hat{L}_0^{-1} \hat{L}_1 - \hat{L}_2 \right) \overset{\text{metal}}{\approx} -\frac{1}{eT} \hat{L}_2 . \quad (3.104)$$

Here, the fact is used that for metals the first term in Eq. (3.104) is negligible and therefore the shown approximation holds [69]. As discussed in Sec. 4.1.1, in this case there exists also a simple relation between the charge and heat conductivity

$$\hat{\kappa} = \frac{\pi^2 k_B^2}{3 e^2} T \hat{\sigma}, \quad (3.105)$$

which is known as WIEDEMANN-FRANZ law [70].

THERMOPOWER (SEEBECK COEFFICIENT)

The SEEBECK effect is a thermoelectric phenomenon, which couples thermal and electronic properties. For this effect usually a sample with open circuit is exposed to a temperature gradient. Due to the open circuit condition there exists no charge current in equilibrium. Instead, the temperature gradient creates a charge accumulation, which can be understood as an induced internal electric field. Both, the temperature gradient as well as the internal electric field cause partial currents, which cancel each other, when the charge accumulation is fully built up.

The size of the SEEBECK effect is described by the thermopower \hat{S} (or SEEBECK coefficient), which relates the temperature gradient to the internal electric field expressed by the charge accumulation

$$\frac{1}{e} \nabla \mu = \hat{S} \nabla T = -\frac{1}{eT} \hat{L}_0^{-1} \hat{L}_1 \nabla T. \quad (3.106)$$

This formula is obtained from Eq. (3.93) under the conditions $E = 0$ and $j = 0$. Finally, the thermopower is given by

$$\hat{S} = -\frac{1}{eT} \hat{L}_0^{-1} \hat{L}_1. \quad (3.107)$$

Within the non-relativistic treatment in literature normally only the diagonal element $S_{xx} = -\frac{1}{eT} \frac{L_{1xx}}{L_{0xx}}$ is considered.

To observe the SEEBECK effect it is common to use an electric circuit of two metals A and B, where their two contact points are exposed to different temperatures. Then, the voltage U measured in the circuit is given by [69]

$$U = \int_{T_1}^{T_2} (S_{xx}^A - S_{xx}^B) dT. \quad (3.108)$$

3.2.3 SPIN HALL EFFECT

For the description of the spin HALL effect the quantization axis for the spins is chosen in z direction. Furthermore, the electric field is assumed to be applied in x direction, which causes a charge current parallel to it. At the same time, a spin current perpendicular to the electric field and to the quantization axis is created. The relations between both currents and the electric field are given by the equations

$$j_x = \sigma_{xx} E_x , \quad (3.109)$$

$$j_y^s = \sigma_{yx}^s E_x . \quad (3.110)$$

Here, σ_{yx}^s is the spin HALL conductivity, which determines the size of the spin HALL effect. However, to describe the efficiency of the spin HALL effect in creating a pure spin current another quantity is used. Namely, this is the spin HALL angle [12]

$$\alpha = \frac{\sigma_{yx}^s}{\sigma_{xx}} , \quad (3.111)$$

the ratio between the spin HALL conductivity and the longitudinal charge conductivity.

TWO-CURRENT DESCRIPTION

The two-current model introduced by MOTT was already mentioned for the description of the spin conductivity in Eq. (3.101) and is discussed here in more detail, since it is important for the calculation of several transport properties. It allows to describe spin-dependent transport phenomena, since it is considered that the scattering processes depend on the spin direction. With the appropriate gauge transformation [63], electrons are separated to spin-up and spin-down channels, where the spins are parallel or antiparallel to the z direction, respectively.

Furthermore, the considered host system has a cubic symmetry and is nonmagnetic. From the symmetry point of view the conductivity tensors for the two spin channels are given by

$$\hat{\sigma}^+ = \begin{pmatrix} \sigma_{xx}^+ & -\sigma_{yx}^+ & 0 \\ \sigma_{yx}^+ & \sigma_{xx}^+ & 0 \\ 0 & 0 & \sigma_{zz}^+ \end{pmatrix} = (\hat{\sigma}^-)^T . \quad (3.112)$$

This relation offers the opportunity to express transport properties only in terms of spin-up quantities. Due to the spin degeneracy provided by space and time inversion symmetry [62], the diagonal elements for the two spin directions are equal, but the off-diagonal elements have the opposite sign [71]. For this reason, the conductivity tensor

$$\hat{\sigma} = \hat{\sigma}^+ + \hat{\sigma}^- = 2 \begin{pmatrix} \sigma_{xx}^+ & 0 & 0 \\ 0 & \sigma_{xx}^+ & 0 \\ 0 & 0 & \sigma_{zz}^+ \end{pmatrix} \quad (3.113)$$

has a diagonal form, while the spin conductivity tensor

$$\hat{\sigma}^s = \hat{\sigma}^+ - \hat{\sigma}^- = 2 \begin{pmatrix} 0 & -\sigma_{yx}^+ & 0 \\ \sigma_{yx}^+ & 0 & 0 \\ 0 & 0 & 0 \end{pmatrix} \quad (3.114)$$

has only off-diagonal elements, which means that spin currents can occur only transverse to an applied electric field.

3.2.4 SPIN NERNST EFFECT

To describe the spin NERNST effect, one can distinguish between two experimental setups, where either a spin accumulation (open circuit case) or a spin current (short circuit case) is created perpendicular to the temperature gradient. As before, the quantization axis is chosen in z direction. Similar to the electric field the temperature gradient is assumed to be applied in x direction: $\nabla T = (\nabla_x T) \mathbf{e}_x$. Then, the spin-dependent transport equation is given by

$$\mathbf{j}^\pm = - \begin{pmatrix} L_{0xx}^+ & \mp L_{0yx}^+ & 0 \\ \pm L_{0yx}^+ & L_{0xx}^+ & 0 \\ 0 & 0 & L_{0zz}^+ \end{pmatrix} \nabla \mu^\pm + \frac{1}{T} \begin{pmatrix} L_{1xx}^+ & \mp L_{1yx}^+ & 0 \\ \pm L_{1yx}^+ & L_{1xx}^+ & 0 \\ 0 & 0 & L_{1zz}^+ \end{pmatrix} (-\nabla T) . \quad (3.115)$$

OPEN CIRCUIT CASE

Let us consider first the open circuit case, which means the system is electrically insulated. Therefore, in equilibrium there exists no resulting charge current or

spin current. Consequently, due to

$$\mathbf{j} = \mathbf{j}^+ + \mathbf{j}^- = 0, \quad \mathbf{j}^s = \mathbf{j}^+ - \mathbf{j}^- = 0, \quad (3.116)$$

both partial current densities \mathbf{j}^\pm are vanishing. This condition allows to define a thermopower \hat{S}^\pm for each spin direction separately, which relates the chemical potential change created by an accumulation of spin-up or spin-down electrons to an applied temperature gradient

$$\frac{1}{e} \nabla \mu^\pm = \hat{S}^\pm \nabla T, \quad \hat{S}^\pm = -\frac{1}{eT} (\hat{L}_0^\pm)^{-1} \hat{L}_1^\pm. \quad (3.117)$$

The total thermopower \hat{S} , which determines the size of the charge accumulation $\nabla \mu$, is defined by the average value of the two spin-dependent thermopowers as

$$\frac{1}{e} \nabla \mu = \frac{1}{2} \frac{1}{e} (\nabla \mu^+ + \nabla \mu^-) = \frac{1}{2} (\hat{S}^+ + \hat{S}^-) \nabla T = \hat{S} \nabla T. \quad (3.118)$$

If instead of the sum the difference of the spin-dependent thermopowers is taken, then the so-called spin SEEBECK coefficient \hat{S}_{yx}^s is obtained [71]

$$\frac{1}{e} \nabla \mu^s = \frac{1}{2} \frac{1}{e} (\nabla \mu^+ - \nabla \mu^-) = \frac{1}{2} (\hat{S}^+ - \hat{S}^-) \nabla T = \hat{S}^s \nabla T, \quad (3.119)$$

which describes the size of the spin accumulation $\nabla \mu^s$.

The tensor structures as well as the relation between the thermopowers for both spin channels are identical to those of the conductivities in Eq. (3.112). Therefore, the total thermopower has only diagonal elements, while the spin SEEBECK coefficient has only off-diagonal elements

$$\hat{S} = \begin{pmatrix} S_{xx} & 0 & 0 \\ 0 & S_{xx} & 0 \\ 0 & 0 & S_{zz} \end{pmatrix}, \quad \hat{S}^s = \begin{pmatrix} 0 & -S_{yx}^s & 0 \\ S_{yx}^s & 0 & 0 \\ 0 & 0 & 0 \end{pmatrix}. \quad (3.120)$$

As was mentioned above, the temperature gradient is chosen in the x direction. Consequently, the charge accumulation occurs only in the x direction due to the SEEBECK effect, while the spin accumulation appears only in the y direction. These accumulations are described by the following two equations

$$\frac{1}{e} \nabla_x \mu = S_{xx} \nabla_x T, \quad (3.121)$$

$$\frac{1}{e} \nabla_y \mu^s = S_{yx}^s \nabla_x T. \quad (3.122)$$

They include the diagonal element of the thermopower

$$S_{xx} = -\frac{1}{eT} \frac{\left(L_{0xx}^+ L_{1xx}^+ + L_{0yx}^+ L_{1yx}^+\right)}{L_{0xx}^{+2} + L_{0yx}^{+2}} \quad (3.123)$$

and the off-diagonal element of the spin SEEBECK coefficient

$$S_{yx}^s = -\frac{1}{eT} \frac{\left(L_{0xx}^+ L_{1yx}^+ + L_{0yx}^+ L_{1xx}^+\right)}{L_{0xx}^{+2} + L_{0yx}^{+2}}, \quad (3.124)$$

respectively. The quantities L_{nxx} are normally significantly larger than the corresponding L_{nyx} . Therefore, the second term of both the numerator and denominator in Eq. (3.123) can be neglected. This leads to the conventional, scalar expression of the thermopower present in the literature $S = -\frac{1}{eT} \frac{L_{1xx}}{L_{0xx}}$ [69]. This means the spin accumulation induced by spin-dependent scattering of the electrons driven by spin-orbit coupling leads to small corrections for the thermopower, which can either slightly enhance or reduce the SEEBECK effect. The simplified formula illustrates, that the SEEBECK effect is strong when the derivative of the conductivity at the FERMI energy is large in comparison to the conductivity itself. In addition, the sign of the thermopower is provided by the sign of the energy derivative of σ_{xx} at the FERMI level.

By contrast, the spin SEEBECK coefficient of Eq. (3.124) is a quantity, which can be only obtained, if the spin-orbit interaction is taken into account. In comparison to S_{xx} , no prediction can be made easily with respect to the contributions of the two terms in the numerator. They are generally quite different between systems. Both terms can independently have either positive or negative signs and in general there is no dominance of one of them. This implies they can add up or cancel each other partly, which makes it difficult to estimate the effect and prohibits an easy explanation.

SHORT CIRCUIT CASE

Let us consider now the case, where the system has a short circuit in the y direction. This leads to a spin current instead of a spin accumulation. An additional charge current in this direction is still impossible due to the special symmetry of

the considered systems as discussed above. Again, in the direction of the temperature gradient the system is assumed to be electrically insulated. As a consequence of the conditions mentioned above, all following quantities vanish: j_x , j_x^s , j_x^\pm , j_y , $\nabla_x \mu^s$, $\nabla_y \mu$, $\nabla_y \mu^s$, $\nabla_y \mu^\pm$. The transport equations, given by Eq. (3.115), reduce to

$$0 = -L_{0xx}^+ \nabla_x \mu^\pm - \frac{1}{T} L_{1xx}^+ \nabla_x T, \quad (3.125)$$

$$j_y^\pm = \mp L_{0yx}^+ \nabla_x \mu^\pm \mp \frac{1}{T} L_{1yx}^+ \nabla_x T. \quad (3.126)$$

With $j_x^s = j_x^+ - j_x^- = -L_{0xx}^+ (\nabla_x \mu^+ - \nabla_x \mu^-) = 0$ it is clear that the accumulation of electrons in x direction is identical for both spin directions. This is a result of the present space and time inversion symmetry of the considered systems. In contrast, in magnetic systems the accumulation for both spin channels would be different leading to an additional spin accumulation along the temperature gradient as in Ref. [18].

From $j_x = 0$ one obtains the thermopower as

$$\frac{1}{e} \nabla_x \mu = \tilde{S}_{xx} \nabla_x T, \quad \tilde{S}_{xx} = -\frac{1}{eT} \frac{L_{1xx}^+}{L_{0xx}^+}, \quad (3.127)$$

which reproduces the conventional expression for the thermopower within the non-relativistic treatment [69].

Since in the short circuit case no spin accumulation is created, instead of the spin SEEBECK coefficient another quantity is needed to describe the strength of the effect. A natural choice is to use a linear coefficient, which connects the temperature gradient and the transverse spin current

$$j_y^s = \sigma_{SN} \nabla_x T. \quad (3.128)$$

This coefficient is called spin NERNST conductivity [71] or alternatively thermo-spin HALL conductivity [72], since the effect is a thermal analog to the spin HALL effect. From Eqs. (3.126) and (3.127) the spin current can be obtained as

$$j_y^s = j_y^+ - j_y^- = -2L_{0yx}^+ \nabla_x \mu - \frac{2}{T} L_{1yx}^+ \nabla_x T = \left(-2e\tilde{S}_{xx} L_{0yx}^+ - \frac{2}{T} L_{1yx}^+ \right) \nabla_x T. \quad (3.129)$$

Therefore, the spin NERNST conductivity consists of two terms

$$\sigma_{SN} = \sigma_{SN}^E + \sigma_{SN}^T = \frac{2}{T} \frac{L_{1xx}^+}{L_{0xx}^+} L_{0yx}^+ - \frac{2}{T} L_{1yx}^+, \quad (3.130)$$

which are distinct contributions via the SEEBECK effect and from the temperature gradient directly. Namely, the first term σ_{SN}^E exists if the system is electrically insulated in direction of the temperature gradient. Under this condition a thermal charge current is compensated by the one created by the charge accumulation. The contribution from the first term in Eq. (3.130) becomes large if the product of thermopower and spin HALL conductivity is high. This implies the spin NERNST effect is propelled by a strong transverse scattering as well as a large SEEBECK effect.

The second term, σ_{SN}^T , represents a direct contribution from the temperature gradient. It is large, if there is a strong slope of the spin HALL conductivity around the FERMI energy. This can be understood in that way that “hot” and “cold” electrons move on average with different velocities and mean free paths. Therefore, they are scattered by a different amount and have different transport properties.

Interestingly, two large contributions to Eq. (3.130) separately do not necessarily provide a pronounced spin NERNST effect. Indeed, if both contributions act in opposite directions the resulting effect can still be negligible.

Similar to the spin HALL angle, one may define a quantity, which describes the efficiency of the spin NERNST effect. It is determined by the conversion of a longitudinal heat current into a transverse spin current. With Eqs. (3.128) and (3.102) the corresponding efficiency

$$\gamma = \frac{j_y^s}{q_x} = \frac{\sigma_{SN}}{-\kappa} \quad (3.131)$$

is obtained. Here, a similarity to the spin HALL effect is also provided by the fact that the heat and charge conductivities are connected by the WIEDEMANN-FRANZ law [70], as discussed in Sec. 3.2.2.

3.2.5 TERNARY ALLOYS - MATTHIESSEN'S RULE

Before, the skew-scattering mechanism for the spin HALL effect was discussed in literature assuming binary dilute alloys [12]. In this work dilute ternary alloys of the form $\text{Cu}(A_{1-w}B_w)$ are also considered consisting of a copper host with two different types of substitutional impurities A and B. The quantity w is a weighting factor, which determines the proportion of both impurity types. The total impurity concentration is fixed to 1 at.%, which allows a description in the dilute limit, where the impurities providing the elastic scattering processes are treated independently from each other.

An approximate way to obtain transport properties of the mentioned ternary alloys is to use MATTHIESSEN'S rule. This rule can be used, when different non-interacting scatterers are present at the same time [73], which can be for example impurities and phonons. Here, scattering at impurity atoms of the type A and B is treated separately. MATTHIESSEN'S rule says that the resistivities of both individual scattering processes add up to the total resistivity. Usually, this assumption holds not exactly, but can give reasonable results [24]. The reason for the deviations of the first-principles results from this rule can be understood with help of the variational principle.

VARIATIONAL PRINCIPLE

The solution of the BOLTZMANN equation, which is a linear inhomogeneous integral equation with a positive self-adjoint kernel, can be found if the variational principle is applied to a trial function. Such a trial function Φ_k is introduced in the linearized ansatz for distribution function

$$f_k = f_k^0 + g_k = f_k^0 - \Phi_k \frac{\partial f_k^0}{\partial \mathcal{E}_k}, \quad (3.132)$$

as was discussed by ZIMAN for a non-relativistic case [73]. For simplicity we consider only one band and therefore the distribution function has only the wave vector as index. Then, the BOLTZMANN equation can be written in the following compact notation

$$X = P\Phi. \quad (3.133)$$

Here, X represents the lefthand side of the BOLTZMANN equation for electrons in an electric field

$$X = -\frac{\partial f_k^0}{\partial \mathcal{E}_k} v_k e E \quad (3.134)$$

and P is the scattering operator in the scattering term

$$P\Phi = \sum_{k'} (P_{k'k} g_{k'} - P_{kk'} g_k) = -\frac{\partial f_k^0}{\partial \mathcal{E}_k} \sum_{k'} (P_{k'k} \Phi_{k'} - P_{kk'} \Phi_k). \quad (3.135)$$

The operator P is linear, self-adjoint and positive definite [73]. With this properties it can be proven that the solution of Eq. (3.133) provides the maximum value of $\langle \Phi, P\Phi \rangle$ in

$$\langle \Phi, P\Phi \rangle = \langle \Phi, X \rangle , \quad (3.136)$$

where the scalar product is defined as $\langle \Phi_a, \Phi_b \rangle = \sum_k \Phi_a(\mathbf{k})\Phi_b(\mathbf{k})$. It follows directly, that

$$\rho = \frac{\langle \Phi, P\Phi \rangle}{\langle \Phi, X \rangle^2} \quad (3.137)$$

adopts its minimal value, which provides the longitudinal resistivity ρ .

If one considers two types of elastic scatterers, the resulting scattering operator is given by the sum of the scattering operators of both contributions

$$P = P_1 + P_2 . \quad (3.138)$$

For the resistivity of the scattering process “1” the following relation

$$\rho_1 \equiv \frac{\langle \Phi_1, P_1\Phi_1 \rangle}{\langle \Phi_1, X \rangle^2} \leq \frac{\langle \Phi, P_1\Phi \rangle}{\langle \Phi, X \rangle^2} \quad (3.139)$$

is valid, because Φ does not have to be a solution of the BOLTZMANN equation corresponding to P_1 . The equality sign only holds, if $\Phi = c\Phi_1$, where c is a constant multiplier. This leads to the following expression

$$\rho \geq \rho_1 + \rho_2 , \quad (3.140)$$

which means that the deviations from MATTHIESSEN’S rule are always positive for the charge conductivity. These deviations are usually small, since due to the variational principle an error of first order for Φ generates only an error of second order for the resistivity [73]. For nonmagnetic dilute ternary alloys, as investigated in this work, the deviations are known to be not drastic [24].

MATTHIESSEN’S RULE FOR THE SPIN CONDUCTIVITY

A next step done in this work is to use MATTHIESSEN’S rule not only for the longitudinal conductivity, but also for the spin HALL conductivity. This point

is much more problematic than can be expected at a first glance. The reason is that MATTHIESSEN'S rule is always applied to resistivities, where the behaviour is always linear between resistivities for each contribution. The calculation of the longitudinal resistivities from the conductivities is rather simple, because both tensors have a diagonal structure. In contrast, the tensor of the spin conductivity in Eq. (3.114) is singular, which makes a calculation of the spin resistivity via matrix inversion $\hat{\rho}^s = (\hat{\sigma}^s)^{-1}$ impossible. To overcome these problems one can apply MATTHIESSEN'S rule (MR) to the spin-dependent resistivities

$$\hat{\rho}^{\pm MR}(w) = (1 - w)\hat{\rho}^{\pm A} + w\hat{\rho}^{\pm B}, \quad (3.141)$$

where $\hat{\rho}^{\pm}$ is the inverse matrix of $\hat{\sigma}^{\pm}$ in Eq. (3.112). Then, the longitudinal charge conductivity and the spin HALL conductivity can be obtained as

$$\sigma_{xx}^{MR} = 2\sigma_{xx}^{+MR} = 2 \frac{\rho_{xx}^{+MR}}{\left(\rho_{xx}^{+MR}\right)^2 + \left(\rho_{yx}^{+MR}\right)^2}, \quad (3.142)$$

$$\sigma_{yx}^{sMR} = 2\sigma_{yx}^{+MR} = -2 \frac{\rho_{yx}^{+MR}}{\left(\rho_{xx}^{+MR}\right)^2 + \left(\rho_{yx}^{+MR}\right)^2}. \quad (3.143)$$

$$(3.144)$$

However, the spin-dependent treatment even leads to small correction of the longitudinal conductivity in comparison to the direct inversion of the diagonal conductivity tensor, where $\sigma_{xx}^{MR} = 2/\rho_{xx}^{+MR}$.

The results of this model will be compared with those of a full ab initio approach considered in Sec. 3.3.1.

MATTHIESSEN'S RULE FOR SPIN NERNST EFFECT

It is also possible to apply MATTHIESSEN'S rule for the description of the spin NERNST effect, but this requires more effort. Here, one needs the energy-dependent conductivity tensor $\hat{\sigma}^+(\mathcal{E})$ of the two constituent binary alloys. For each energy MATTHIESSEN'S rule is applied to calculate the longitudinal and HALL conductivity of the ternary alloy as explained in the previous section. The energy integration has to be performed for each considered weighting factor w to obtain the transport coefficient \hat{L}_n^+ similar to Eq. (3.95). At the end, the spin NERNST conductivity, the

heat conductivity, and the efficiency of the NERNST effect can be calculated just from quantities of the binary alloys.

3.3 TECHNICAL REMARKS

3.3.1 TRANSPORT KKR CODE FOR TERNARY ALLOYS

In addition to MATTHIESSEN'S rule the transport KKR was used to obtain more precise results for the ternary alloys. This was done by calculating the microscopic transition probability for a ternary alloy via adding the corresponding quantities of the constituent binary alloys

$$P_{kk'}^{AB}(w) = (1 - w)P_{kk'}^A + wP_{kk'}^B . \quad (3.145)$$

This required the following modifications in the KKR code:

The starting point is that the host GREEN function \hat{G} , the defect GREEN function G , and the difference of the single-site t-matrices between the defect and the host system, denoted by t , were obtained for the corresponding binary alloys. Since these three quantities are connected via the DYSON equation, it is sufficient to have either just \hat{G} and t or G and t of both systems. To reduce the computational effort in the transport KKR code, the first possibility was chosen, because only one GREEN function is needed in this case. Following from this the defect-matrix of Eq. (3.66), the transition matrix of Eq. (3.79), and the microscopic transition probability of Eq. (3.85) were calculated for each binary alloy separately. From those the transition probabilities were combined according to Eq. (3.145). Finally, the transport properties were calculated as usual with the iterative solution of the linearized BOLTZMANN equation, Eq. (3.89).

However, the used method does not allow a fast calculation of the transport properties in the whole range of $w \in [0, 1]$ as MATTHIESSEN'S rule from Eq. (3.141) does. Instead, for each value of w a separate full transport calculation has to be performed. Therefore, the first principles results were obtained only for several chosen values of w .

3.3.2 INTEGRATION OVER THE ENERGY

An important point for the description of the spin NERNST effect is an accurate calculation of the linear transport coefficients

$$\hat{L}_n(T) = -\frac{1}{e} \int \hat{\sigma}(\mathcal{E}) \left(-\frac{\partial f^0(\mathcal{E}, T)}{\partial \mathcal{E}} \right) (\mathcal{E} - \mu)^n d\mathcal{E} , \quad n = 0, 1, 2 . \quad (3.146)$$

This requires the conductivity as a function of the energy. Fortunately, this quantity is multiplied with the energy derivative of the FERMI function, which decays exponentially with distance from the FERMI energy. Fig. 3.1 shows the typical behaviour of the functions $(-\partial f^0 / \partial \mathcal{E})(\mathcal{E} - \mathcal{E}_F)^n$, which together with $\sigma(\mathcal{E})$ provide the integrand. Therefore, it is sufficient to calculate $\hat{\sigma}(\mathcal{E})$ in a small energy inter-

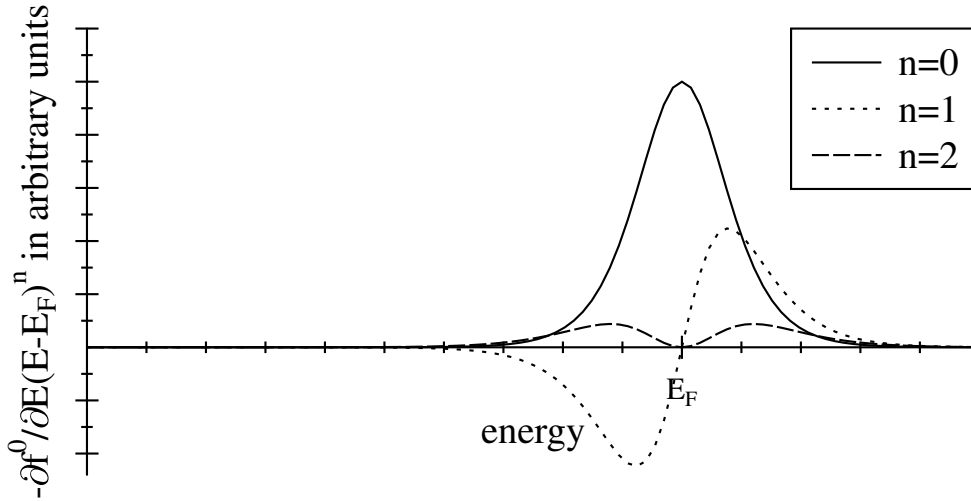


Figure 3.1: The typical behaviour of the functions $(-\partial f^0 / \partial \mathcal{E})(\mathcal{E} - \mu)^n$ with $n=0, 1, 2$ is shown.

val around the FERMI energy. The necessary size of the interval depends on the temperature at which $\hat{L}_n(T)$ is needed. Inside this interval an energy mesh is created. If chosen wisely, it can be used for different temperatures as explained in the following. In this work transport properties between 30K and 300K are presented. The maximal temperature determines the size of our energy interval, which was chosen in the way that

$$\int_{\mathcal{E}_{min}}^{\mathcal{E}_{max}} \left(-\frac{\partial f^0}{\partial \mathcal{E}} \right) d\mathcal{E} > 0.9999 . \quad (3.147)$$

This is valid for $\mathcal{E}_{min} = \mathcal{E}_F - 0.02Ry < \mathcal{E} < \mathcal{E}_F + 0.02Ry = \mathcal{E}_{max}$. In this interval it is necessary to have most of the energy points close to \mathcal{E}_F , since the main contribution

to the integral comes from the central area particularly for 30K. Furthermore at least some points which are less dense further away from \mathcal{E}_F are needed. They are necessary to determine the contributions from a slower decaying derivative of the FERMI function at 300K.

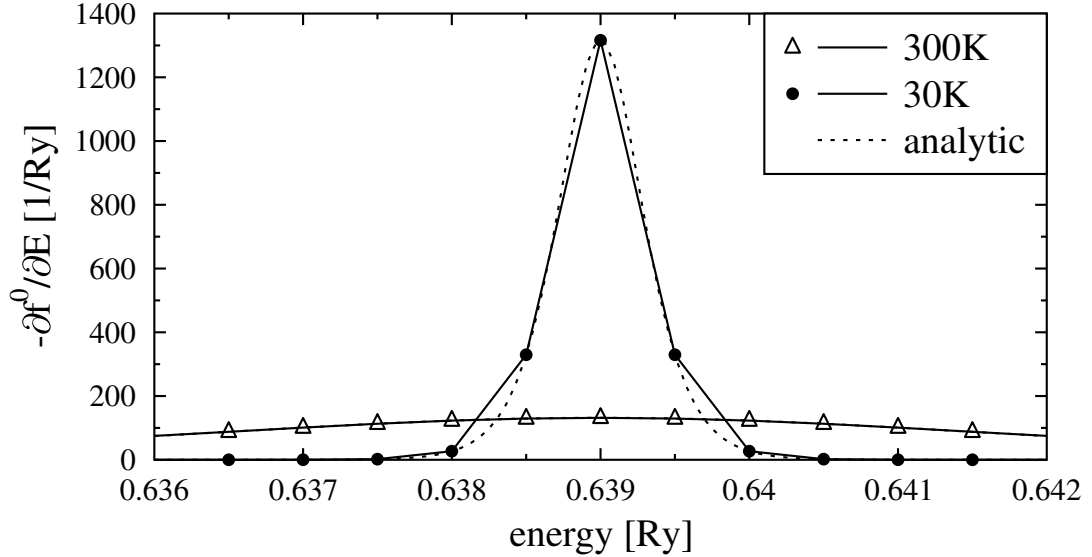


Figure 3.2: Description of $(-\partial f^0/\partial \mathcal{E})$ at 300K and 30K via the chosen energy mesh and corresponding analytic functions at the center of the chosen energy interval.

The central region of the chosen energy mesh is shown in Fig. 3.2 to illustrate how well the derivative of the FERMI function is approximated. While the curve for 300K looks quite smooth one can easily see that for 30K probably some parts will be missing during the integration. To improve this situation the following procedure is applied: Before the multiplication of $\hat{\sigma}(\mathcal{E})$ with $(-\partial f^0/\partial \mathcal{E})(\mathcal{E} - \mu)^n$ the energy mesh for $\hat{\sigma}(\mathcal{E})$ is refined. Between each pair of adjacent energy points 9 additional equidistant points are created for which $\hat{\sigma}(\mathcal{E})$ is determined via a linear interpolation. Afterwards, the integral of Eq. (3.146) is approximated by a simple trapezoidal rule. To prove that the refined energy mesh is sufficient, the condition of Eq. (3.147) was used.

4 RESULTS

In this chapter different transport properties describing spin-transport phenomena in Cu-based dilute alloys with nonmagnetic impurities are discussed. First, the spin NERNST effect is investigated in alloys with only one type of impurity. Two cases leading either to a spin accumulation or spin current are considered. In the following, results for the spin HALL effect and spin NERNST effect are presented for ternary alloys, consisting of a Cu host with two types of impurities. It is checked whether MATTHIESSEN'S rule, where the scattering at both types of impurities is treated independently, can provide reasonable results. Furthermore, the general behaviour of the spin HALL conductivity and spin HALL angle is investigated analytically within the approximation of MATTHIESSEN'S rule. Finally, it is studied, whether the efficiencies of the spin HALL and spin NERNST effect can be enhanced in a ternary alloy with respect to the constituent binary alloys.

4.1 SPIN NERNST EFFECT IN BINARY ALLOYS

To obtain the transport properties for the spin NERNST effect at first the conductivity tensor for spin-up electrons was calculated for different energies in a small interval around the FERMI energy. The values of the longitudinal and transversal component are presented in Fig. 4.1 for a Cu host with Au, Ti, Bi, or Zn impurities. From these data the general transport coefficients, shown in Table 4.1 for room temperature, were calculated. The table in combination with the figure demonstrates, that the size and the sign of the components of \hat{L}_0^+ are correlated with those of $\hat{\sigma}^+(\mathcal{E}_F)$. This is a consequence of the almost linear behaviour of the conductivity in the considered energy interval. Indeed, as shown by Eq. (4.2) in Sec. 4.1.1, \hat{L}_0^+ is simply proportional to $\hat{\sigma}^+(\mathcal{E}_F)$ in such a case. In contrast, according to Eq. (4.4) the components of \hat{L}_1^+ are proportional to the energy derivatives of the corresponding conductivities at \mathcal{E}_F . Therefore, the sign and the magnitude of

L_{1xx}^+ and L_{1yx}^+ are determined by the slope of the longitudinal and HALL conductivity, respectively. From these general transport coefficients all transport properties, which are required to describe the spin NERNST effect, can be expressed.

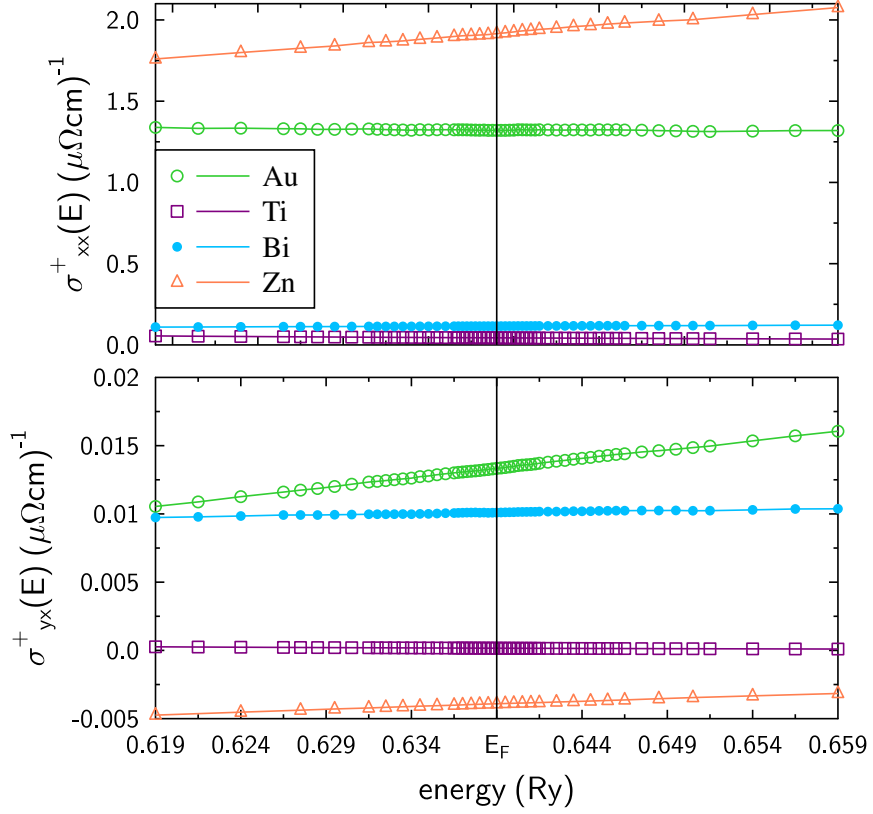


Figure 4.1: Longitudinal and transversal components of the energy-dependent conductivity tensor for spin-up electrons, which are calculated for Cu(Au), Cu(Ti), Cu(Bi), and Cu(Zn) alloys. The impurity concentration in the Cu host is 1 at.%.

4.1.1 OPEN CIRCUIT CASE

At first the open circuit case is treated, where neither macroscopic charge nor spin currents can flow in the stationary state. Instead, a charge accumulation

imp	L_{0xx}^+ (1/Vms)	L_{0yx}^+ (1/Vms)	L_{1xx}^+ (A/m)	L_{1yx}^+ (A/m)
Au	-8.26×10^{26}	-8.33×10^{24}	3.20×10^3	-2.27×10^3
Ti	-2.73×10^{25}	-1.01×10^{23}	7.64×10^3	6.37×10^1
Bi	-7.23×10^{25}	-6.31×10^{24}	-5.18×10^3	-3.01×10^2
Zn	-1.20×10^{27}	2.44×10^{24}	-1.35×10^5	-6.21×10^2

Table 4.1: Longitudinal and transversal components of the general transport coefficients at 300 K for a Cu host with an impurity concentration of 1 at.%.

in direction of the temperature gradient and a spin accumulation transverse to it are generated. These accumulations are proportional to the thermopower and to the spin SEEBECK coefficient given by the Eqs. (3.123) and (3.124), respectively. Figure 4.2 shows their almost linear behaviour as functions of the temperature. This is caused by the nearly linear behaviour of the energy-dependent conductivity tensor in the considered energy interval, as shown in Fig. 4.1. Indeed, if one assumes for the conductivity

$$\hat{\sigma}^+(\mathcal{E}) = \hat{\sigma}^+(\mathcal{E}_F) + (\mathcal{E} - \mathcal{E}_F) \left. \frac{d\hat{\sigma}^+(\mathcal{E})}{d\mathcal{E}} \right|_{\mathcal{E}=\mathcal{E}_F}, \quad (4.1)$$

then the quantity

$$\hat{L}_0^+(T) = -\frac{1}{e} \int d\mathcal{E} \hat{\sigma}^+(\mathcal{E}_F) \left(-\frac{\partial f^0}{\partial \mathcal{E}} \right) = -\frac{1}{e} \hat{\sigma}^+(\mathcal{E}_F) \quad (4.2)$$

is temperature independent. In contrast, the quantity

$$\hat{L}_2^+(T) = -\frac{1}{e} \int d\mathcal{E} (\mathcal{E} - \mathcal{E}_F)^2 \hat{\sigma}^+(\mathcal{E}_F) \left(-\frac{\partial f^0}{\partial \mathcal{E}} \right) = -\frac{1}{e} \frac{\pi^2}{3} (k_B T)^2 \hat{\sigma}^+(\mathcal{E}_F), \quad (4.3)$$

shows a quadratic behaviour, but is also only determined by the first term of Eq. (4.1). With this equation the WIEDEMANN-FRANZ law in Eq. (3.105) is confirmed. If this procedure is applied to $\hat{L}_1^+(T)$ by solving SOMMERFELD integrals again a quadratic behaviour

$$\hat{L}_1^+(T) = -\frac{1}{e} \int d\mathcal{E} (\mathcal{E} - \mathcal{E}_F)^2 \left. \frac{d\hat{\sigma}^+(\mathcal{E})}{d\mathcal{E}} \right|_{\mathcal{E}=\mathcal{E}_F} \left(-\frac{\partial f^0}{\partial \mathcal{E}} \right) = -\frac{1}{e} \frac{\pi^2}{3} (k_B T)^2 \left. \frac{d\hat{\sigma}^+(\mathcal{E})}{d\mathcal{E}} \right|_{\mathcal{E}=\mathcal{E}_F}$$

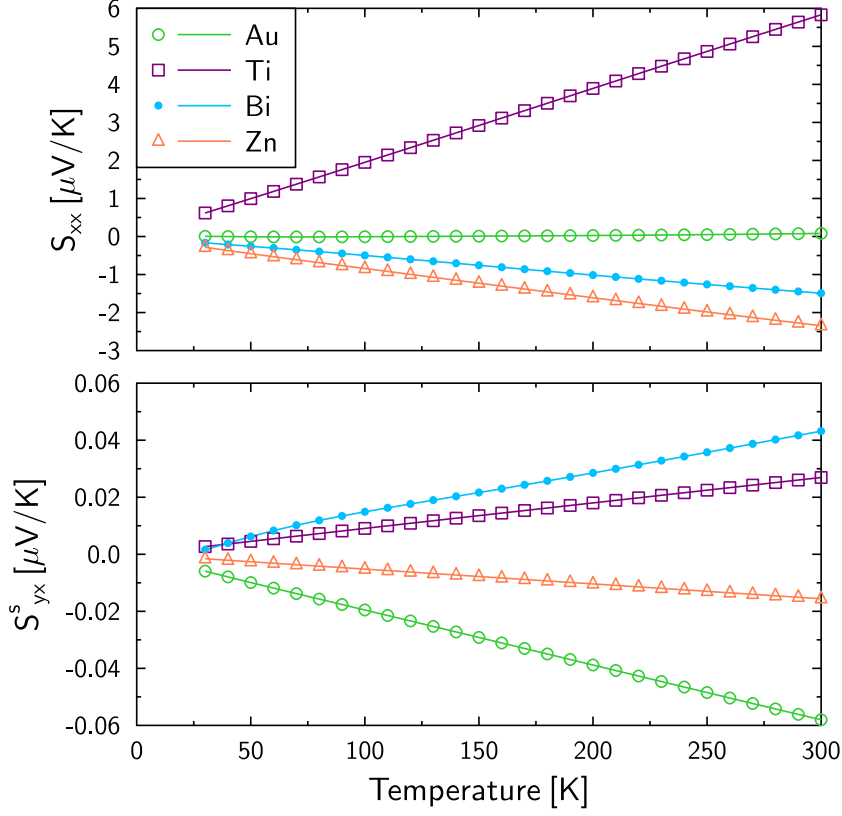


Figure 4.2: Longitudinal component of the thermopower and off-diagonal component of the spin SEEBECK coefficient.

(4.4)

is obtained and the quantity is proportional to the derivative of $\hat{\sigma}^+(\mathcal{E})$ at the FERM level. As a result, the quantities S_{xx} and S_{yx}^s become linear functions with respect to the temperature. For example, it can be easily seen from Eq. (3.123) that the thermopower is linear with respect to T :

$$S_{xx} \approx -\frac{1}{eT} \frac{L_{1xx}^+}{L_{0xx}^+} \propto \frac{1}{T} \frac{T^2}{const.} \propto T. \quad (4.5)$$

A further interesting point provided in Fig. 4.2 is that the thermopower and the spin SEEBECK coefficient strongly depend on the impurity type. Especially, the

thermopower differs by two orders of magnitude between the Cu(Au) and Cu(Ti) alloy. Furthermore, there is obviously no simple correlation between S_{xx} and S_{yx}^s , which is also in agreement with the discussion of the Eqs. (3.123) and (3.124) in Sec. 3.2.4. This implicates that a strong SEEBECK effect does not necessarily leads to a large transverse spin accumulation. Moreover, even the direction of the charge and spin accumulation is independent from each other. With the considered alloys all four possible combinations of signs are found for S_{xx} and S_{yx}^s .

4.1.2 SHORT CIRCUIT CASE

Now the second case is considered, where it is allowed that a transverse spin current is flowing, which is created instead of the spin accumulation. In direction of the temperature gradient the open circuit condition is kept, which still leads to a longitudinal charge accumulation. However, this charge accumulation is different from the open circuit case, since the thermopower is described by Eq. (3.127) instead of Eq. (3.123). This is the result of the transverse spin current and absence of the corresponding spin accumulation.

imp	\tilde{S}_{xx} of Eq. (3.127) in $\mu V/K$	S_{xx} of Eq. (3.123) in $\mu V/K$	$\frac{ \tilde{S}_{xx}-S_{xx} }{S_{xx}}$ in %
Au	0.08064	0.08005	0.737
Ti	5.82965	5.82975	0.002
Bi	-1.49171	-1.48795	0.253
Zn	-2.34613	-2.34609	0.002
	short circuit	open circuit	

Table 4.2: Thermopower for the open (S_{xx}) and short (\tilde{S}_{xx}) circuit case and absolute value of the relative deviation between both at 300 K.

Comparing the thermopowers for both experimental setups, given in Table 4.2, one can see that the flowing spin current changes the charge accumulation by a small amount of less than 1%. The strength of the SEEBECK effect is slightly decreased for the Cu(Ti) alloy and increased for the three other types of impurity. However, this tiny change of the thermopower can be neglected in practice.

The size of the generated spin current is described by the spin NERNST conductivity, which consists, similar to the spin SEEBECK coefficient in Eq. (3.124), of two

terms:

$$\sigma_{SN} = \sigma_{SN}^E + \sigma_{SN}^T = \frac{2}{T} \frac{L_{1xx}^+}{L_{0xx}^+} L_{0yx}^+ - \frac{2}{T} L_{1yx}^+ . \quad (4.6)$$

If one takes into account $L_{0xx}^+ \approx -\sigma_{xx}^+(\mathcal{E}_F)/e$ and $|L_{0xx}^+| \gg |L_{0yx}^+|$, a simple relation between the spin NERNST conductivity and the spin SEEBECK coefficient can be found:

$$\sigma_{SN} \approx -2\sigma_{xx}^+(\mathcal{E}_F)S_{yx}^s . \quad (4.7)$$

This relation shows that systems, which have a comparably strong spin accumulation like the Cu(Au) and Cu(Bi) alloys, can generate spin currents of different size. Namely, the spin NERNST conductivity for the Cu(Au) alloy is one order of magnitude higher than for the Cu(Bi) alloy, as it is shown in Fig. 4.3. This is caused by the larger longitudinal conductivity of the Cu(Au) alloy, according to Fig. 4.1. However, the sign of the spin NERNST conductivity is always opposite to the spin SEEBECK coefficient, as follows from Eq. (4.7).

In general, Fig. 4.3 shows that the spin NERNST conductivity can be tuned up to three orders of magnitude using different types of substitutional impurities, which can even provide different signs for this quantity.

Let us now discuss the mechanism of two contributions to the spin NERNST conductivity, which are schematically visualized in Fig. 4.4. The contribution from the second term $\sigma_{SN}^T = -\frac{2}{T}L_{1yx}^+$ can be understood quite easily. One can say that this term gives the direct contribution from the temperature gradient, since considering a short circuit condition in the x direction one would obtain $\sigma_{SN} = \sigma_{SN}^T$. Clearly, σ_{SN}^T is proportional to the derivative of the spin HALL conductivity around the FERMI energy. It can be interpreted in such a way, that electrons at the “hot” and at the “cold” side of the sample have on average different velocities and mean free paths. Therefore, the corresponding transport properties are different at both sides. Due to the temperature gradient a longitudinal heat current is flowing. This results in an exchange of electrons with different transport properties, whose inequality leads to an asymmetry of the transverse scattering processes for “hot” and “cold” electrons.

The term σ_{SN}^E is more complicated to understand and occurs only, if in the x direction an open circuit condition holds. It can be expressed with help of the thermopower

$$\sigma_{SN}^E = -2e\tilde{S}_{xx}L_{0yx}^+ . \quad (4.8)$$

This means that this term gives a large contribution, when a material has a strong **SEEBECK** effect in combination with a high spin HALL conductivity. It is schematically visualized on the lefthand side in Fig. 4.4 that due to the charge accumulation there are more electrons at one side of the sample than on the other. This creates internally a longitudinal electric field, which in analogy to the spin HALL effect leads to a transverse spin-dependent scattering to the lateral sides. Finally, the

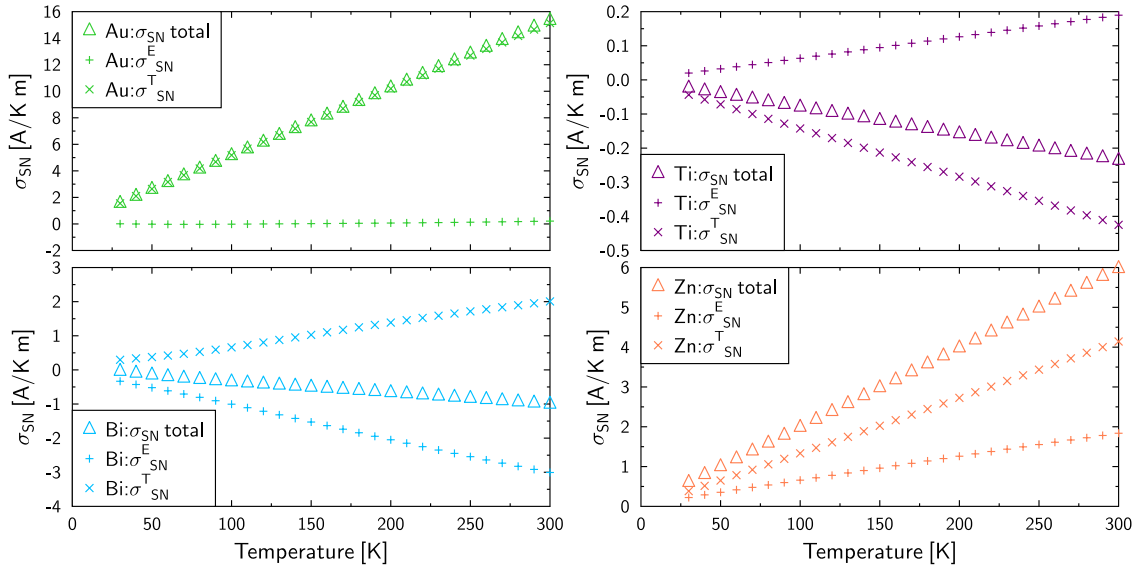


Figure 4.3: Spin NERNST conductivity and its two contributions for Au, Ti, Bi, and Zn impurities in a Cu host at an impurity concentration of 1 at.%.



Figure 4.4: Mechanisms of the two contributions to σ_{SN} .

asymmetric scattering results in a spin current, which is proportional to the spin HALL conductivity.

Since the signs of the quantities L_{0yx}^+ , L_{1xx}^+ , and L_{1yx}^+ are independent of each other, the two contributions to the spin NERNST conductivity can have either the same or the opposite sign. In the latter case, both contributions compensate each other partly, which leads to a reduced total effect. The preferred case is of course, when σ_{SN}^E and σ_{SN}^T add up. For the considered alloys both situations were observed, as it is shown in Fig. 4.3. For the Cu(Ti) and Cu(Bi) alloy relatively small spin NERNST conductivities are obtained, because both contributions itself are small and in addition counteractive. For the other two alloys, where both contributions accumulate, the values are much higher. However, for the Cu(Au) alloy, which has the highest obtained spin NERNST conductivity of about 16 A/Km at 300 K, the term σ_{SN}^T definitely provides the dominant contribution.

EFFICIENCY OF THE SPIN HALL AND SPIN NERNST EFFECT

Here, the efficiencies of both effects are compared, which are presented in Tab. 4.3 for the considered alloys. It is well visible, that both efficiencies are not proportional to each other and even their signs are not related. This can be understood from the formulas, which are used for the calculation of α and γ given by the Eqs. (3.111) and (3.131), respectively. Here, the spin HALL angle α describes the charge to spin current conversion and is defined by the ratio of the spin HALL conductivity and the longitudinal charge conductivity. Similarly, the efficiency of the heat to spin current conversion of the spin NERNST effect is determined by the ratio of the spin NERNST conductivity and heat conductivity, which are shown in Fig. 4.5. Due to the WIEDEMANN-FRANZ law [70] the denominators in the Eqs. (3.111) and (3.131) are proportional to each other. However, this is not the case for the corresponding numerators. In fact, the spin HALL conductivity is included in the spin NERNST conductivity in Eq. (3.130) via the quantity L_{0yx}^+ , but is weighted with the thermopower, which can also influence the sign of the quantity. Furthermore, also the derivative of the spin HALL conductivity is contributing as well. Therefore, it is reasonable that the ratio of α and γ can vary strongly with the impurity type. However, according to Tab. 4.3 there seems to be a trend that alloys with a strong spin HALL effect also provide a strong spin NERNST effect.

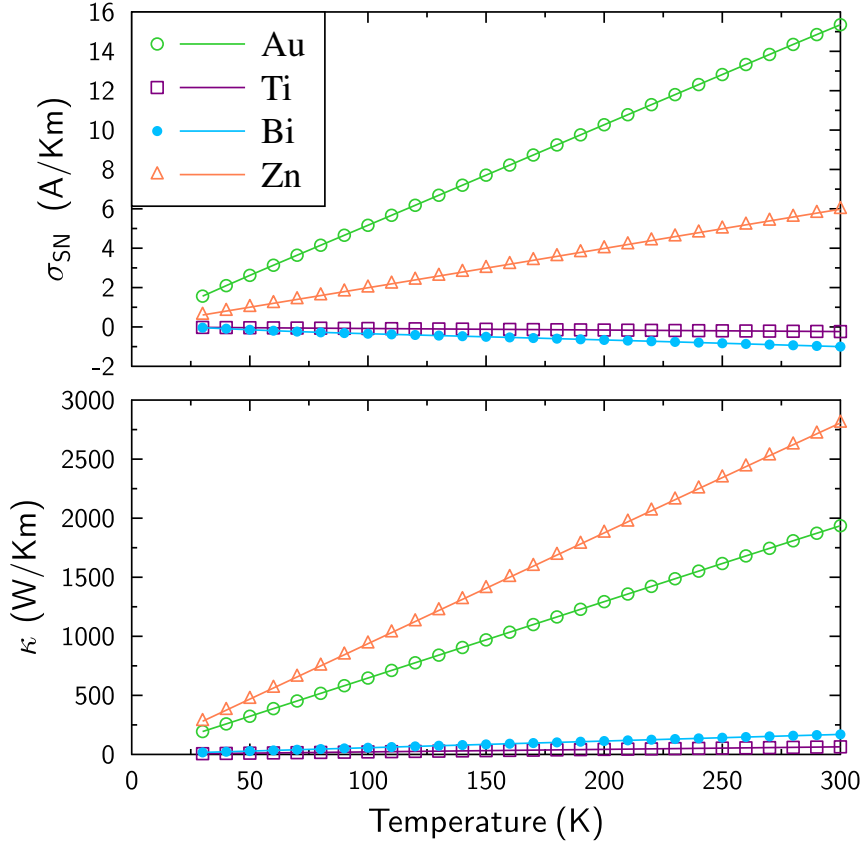


Figure 4.5: Spin NERNST conductivity and heat conductivity for Au, Ti, Bi, and Zn impurities in a Cu host at an impurity concentration of 1 at.%.

imp	α (10^{-3})	γ ($10^{-31}/V$)
Au	10.01	-7.93
Ti	3.71	3.67
Bi	86.56	5.90
Zn	-2.04	-2.13

Table 4.3: Efficiency of the spin HALL effect α and spin NERNST effect γ at 300 K for a Cu host with different substitutional impurities.

EXPECTED CURRENTS

Here, it is presented, how large the spin currents created via the spin NERNST effect can be in comparison to the spin HALL effect. These spin currents depend on the size of the system, the applied temperature gradient and the material properties. For the estimation a sample size of $100 \times 100 \times 100 \text{ nm}$ is assumed, which is the typical dimension for spin HALL devices [11]. Recent thermoelectric experiments have shown, that it is possible to create temperature gradients up to $50 \frac{\text{K}}{\mu\text{m}}$ [23]. Of course, it could be problematic to maintain this temperature gradient, since Cu has a quite high heat conductivity. However, heating via short laser pulses [74] is a promising method to obtain high temperature gradients for short times. The highest calculated spin NERNST conductivity neglecting the spin-flip scattering was found for the Cu(Au) alloy with a value of $\sigma_{SN} = 15.4 \frac{\text{A}}{\text{Km}}$. Under the above mentioned conditions a spin current density of

$$j^s = \sigma_{SN} \nabla T = 15.4 \frac{\text{A}}{\text{Km}} 50 \cdot 10^6 \frac{\text{K}}{\text{m}} \approx 10^9 \frac{\text{A}}{\text{m}^2} \quad (4.9)$$

is obtained. For the considered sample size this leads to a spin current of

$$I_s = 10^9 \frac{\text{A}}{\text{m}^2} \cdot (100 \cdot 10^{-9} \text{m})^2 = 10 \mu\text{A} . \quad (4.10)$$

Since in the dilute limit the spin NERNST conductivity scales linearly with the impurity concentration, with 0.1 at.% of impurity atoms a spin current in the order of about $100 \mu\text{A}$ should be reached. This is already large enough to switch a nanomagnet, as shown in recent experiments [75]. For the considered Cu(Au) alloy with 0.1 at.% of impurity atoms a charge current density of about

$$j = \frac{j^s}{\alpha} = \frac{10^{10} \frac{\text{A}}{\text{m}^2}}{10^{-2}} = 10^{12} \frac{\text{A}}{\text{m}^2} \quad (4.11)$$

would be needed to obtain the equal spin current density via the spin HALL effect. However, this is already close to the electromigration regime [23] and therefore an experimental observation is comparably challenging.

In general, the necessary temperature gradients to obtain reasonable spin currents are quite high. This means on the other hand that accidental temperature gradients, which are normally several orders of magnitude smaller than $50 \frac{\text{K}}{\mu\text{m}}$, will not affect spin HALL experiments, because the created spin NERNST current is negligible in comparison to the spin HALL current.

4.2 INFLUENCE OF SPIN-FLIP SCATTERING AND THE ACCURACY OF THE FERMI SURFACE INTEGRATION

So far, in the considerations spin-flip scattering was excluded. To investigate its influence on the results, corresponding calculations were performed. Furthermore, a comparison with results of S. WIMMER et al. [76] and experimental data [77] was done, which shows a good agreement for most quantities according to Tab. 4.4. However, especially the thermopower in Ref. [76] for the Cu(Au) alloy was found to be about 18 times larger. Such a large value was obtained via the KUBO formalism, where spin-flip scattering is included. Therefore, with the additional calculations it could be tested, whether the discrepancy is caused by these scattering processes. The results for some selected quantities are presented in Fig. 4.6. Here, the blue bars refer to the results published in Ref. [71] and considered in the preceding sections. For the calculations related to the green bars additionally spin-flip processes were included, as was also done in Ref. [76]. Finally, for the red bars the number of k points for the FERMI surface integration was increased to improve the convergence. For easy comparison all quantities are normalized to the latter calculation. One can see that the influence for the improved calculation schemes ranges from negligible for the Cu(Ti) alloy to significant for the Cu(Au) alloy. For all alloys the behaviour of σ_{xx} and κ is similar, since they are connected via WIEDEMANN-FRANZ law [70]. There is also a clear correlation between σ_{5N} and S_{yx}^s , since they are simply related via the longitudinal conductivity, as shown in Eq. (4.7). For the discussion, one can therefore just concentrate on the first four quantities in Fig. 4.6. Whereas the difference in the number of k points has almost no influence on the conductivities, both quantities are decreased for the Cu(Au) and Cu(Bi) alloys, if spin-flip scattering is included. Namely, σ_{xx} is reduced by 11% and 5% while σ_{yx}^s is decreased by 28% and 10% for the Cu(Au) and Cu(Bi) alloys, respectively. The influence is stronger for the spin HALL conductivity than for the longitudinal conductivity, which is reasonable taking into account the nature of σ_{yx}^s . The behavior of the thermopower is totally different from the one of σ_{xx} . Here only the number of k points has a significant effect, especially for the Cu(Au) alloy. This can be understood from the approximated thermopower in Eq. (3.127) together with the definition of the linear transport coefficients in Eq. (3.95). Namely, one can assume that the conductivity is reduced by the same factor for all energies due to spin-flip scattering. Then, this factor cancels out in the thermopower, because it is included in the numerator and denominator. The

influence of the increased number of k points is particularly strong for S_{xx} of the Cu(Au) alloy, because the derivative of the longitudinal conductivity around the FERMI energy is quite small in comparison to the conductivity itself. Therefore, even small relative errors of $\sigma_{xx}(\mathcal{E})$ can lead to big changes in the quantity L_{1xx} . With more k points our result for the thermopower gets closer to the one of Ref. [76], but is still one order of magnitude smaller. However, this difference is not caused by lack of convergence, since the conductivity is sufficiently converged for the high number of k points, as presented in the Figs. 4.7 and 4.8. Furthermore, Fig. 4.7 shows that the energy-dependent conductivity is a quite smooth curve for the calculations with the high number of k points and therefore a further refinement of the k -mesh would not change the thermopower. Instead, the discrepancy seems to be caused by the different treatment of the phenomenon between the quantum mechanical KUBO formalism and the presented semiclassical approach. A main difference is that instead of treating the impurity embedded in a real cluster of host atoms, the KUBO formalism uses the coherent potential approximation [76]. There, the scattering properties at each atomic position are considered as a superposition of those from host material and impurity.

In contrast to S_{xx} , the quantity S_{yx}^s for the Cu(Au) alloy is only influenced by the spin-flip scattering. This is caused by the fact that the term containing L_{1xx} is negligible for this system and the problem with the small derivative does not occur for L_{1yx} . The influence of the spin-flip scattering is caused by the spin HALL conductivity, which is stronger decreased than the longitudinal conductivity.

In general, it was found that the improvement of the calculation parameters has no big influence on the investigated quantities except for the Cu(Au) alloy, discussed above.

imp	$\sigma_{xx}(\mathcal{E}_F)$			$\sigma_{yx}^s(\mathcal{E}_F)$		$S_{xx}(300K)$	
	exp.	Boltz.	Kubo	Boltz.	Kubo	Boltz.	Kubo
Au	1.92	2.64	2.28	2.67×10^{-2}	2.11×10^{-2}	0.08	1.41
Ti	0.12	0.09	0.08	3.24×10^{-4}	4.28×10^{-4}	5.83	5.72
Bi	0.20	0.23	0.19	2.02×10^{-2}	2.05×10^{-2}	-1.49	-1.02

Table 4.4: Longitudinal charge conductivity and spin HALL conductivity in $(\mu\Omega cm)^{-1}$ and thermopower in $\mu V/K$ obtained via Boltzmann approach [71] excluding spin-flip scattering and Kubo formalism [76]. In addition, for the charge conductivity experimental values are given [77].

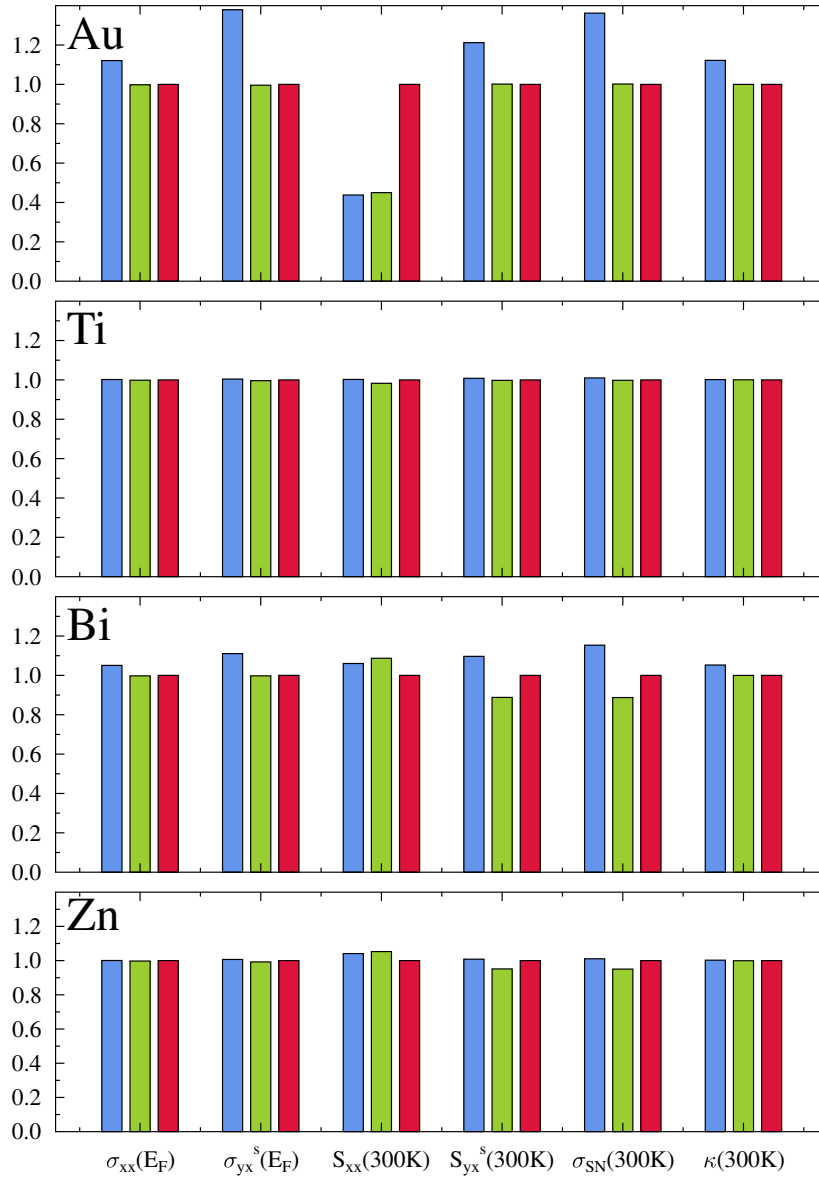


Figure 4.6: Longitudinal conductivity, spin HALL conductivity, thermopower, spin SEEBECK coefficient, spin NERNST conductivity, and heat conductivity for a Cu host with 1 at.% of substitutional Au, Ti, Bi, or Zn impurities. Three different calculation modes were used: without spin-flip scattering and low number of k points for the FERMI surface integration (blue), with spin-flip scattering and low number of k points (green), and with spin-flip scattering and high number of k points (red).

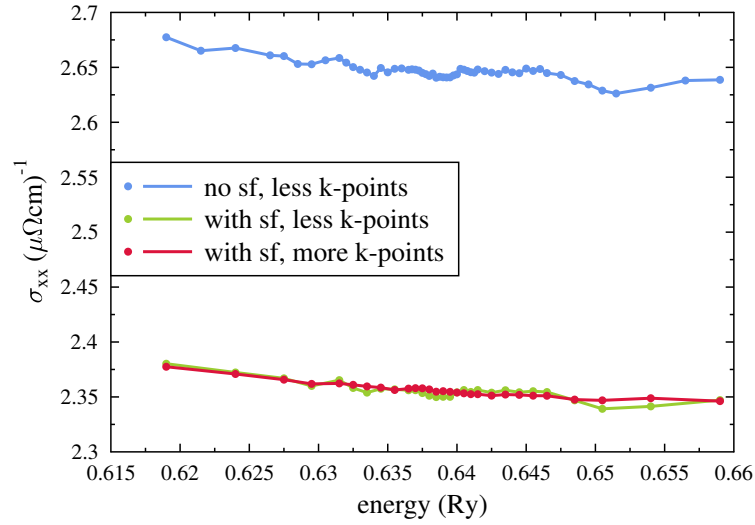


Figure 4.7: Energy dependence of the longitudinal conductivity of the Cu(Au) alloy with three different calculation modes: without spin-flip scattering and low number of k points for the FERMI surface integration (blue), with spin-flip scattering and low number of k points (green), and with spin-flip scattering and high number of k points (red).

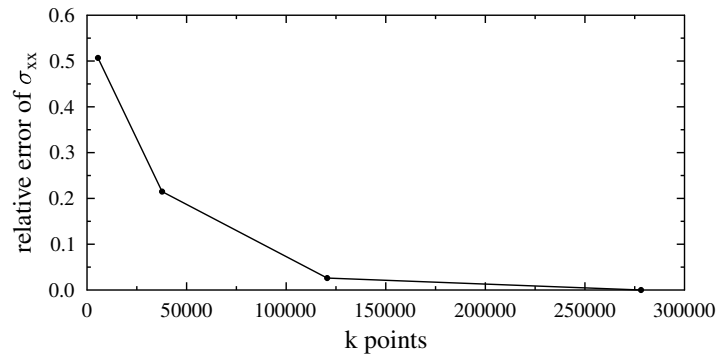


Figure 4.8: Relative error for the longitudinal conductivity of the Cu(Au) alloy as a function of the number of k points with respect to the calculation with the highest number of k points (red curve in Fig. 4.7) for the FERMI surface integration.

4.3 VALIDITY OF MATTHIESSEN'S RULE FOR THE LONGITUDINAL RESISTIVITY & HALL RESISTIVITY

The aim of this section is to test the accuracy of MATTHIESSEN'S rule in comparison to full ab initio calculations. It is known that the relative deviations from this rule are always positive for the longitudinal resistivity [24], but it is of further interest to investigate the nature of such deviations for the HALL resistivity.

For this purpose, at first alloys of the form $\text{Cu}(\text{A}_{0.5}\text{B}_{0.5})$ with two different types of impurities A and B are considered. For the full calculations the method described in Sec. 3.3.1 was used to obtain the conductivity tensor for spin-up electrons. Via matrix inversion the corresponding longitudinal resistivity ρ_{xx}^{+AB} and HALL resistivity ρ_{yx}^{+AB} were obtained. To apply MATTHIESSEN'S rule, the resistivities of the two binary alloys $\text{Cu}(\text{A})$ and $\text{Cu}(\text{B})$ were calculated from the corresponding $\hat{\sigma}^+$ tensor. For the considered ternary alloys MATTHIESSEN'S rule (MR) predicts the resistivities as

$$\rho_{ix}^{+MR} = \frac{1}{2} \left(\rho_{ix}^{+A} + \rho_{ix}^{+B} \right), \quad i = x, y. \quad (4.12)$$

The relative deviations of the full calculations from this rule are defined by

$$\frac{\Delta\rho_{ix}^+}{\rho_{ix}^+} = \frac{\rho_{ix}^{+AB} - \rho_{ix}^{+MR}}{\rho_{ix}^{+MR}}, \quad i = x, y. \quad (4.13)$$

These quantities are presented in Fig. 4.9 for several combinations of non-magnetic impurities. The figure shows that the maximal relative deviations are about 15%, but most values are below 5%. It suggests that MATTHIESSEN'S rule is a good estimation of the transport properties for the considered ternary alloys. The reason for this is the almost spherical FERMI surface of copper, since for spherical bands MATTHIESSEN'S rule holds exactly [73].

As expected according to Ref. [73], the relative deviations of the longitudinal resistivity, shown in the upper left half of the figure, are positive for all considered combinations of impurities. However, the deviations show both signs for the HALL resistivity, presented in the lower right half of the figure.

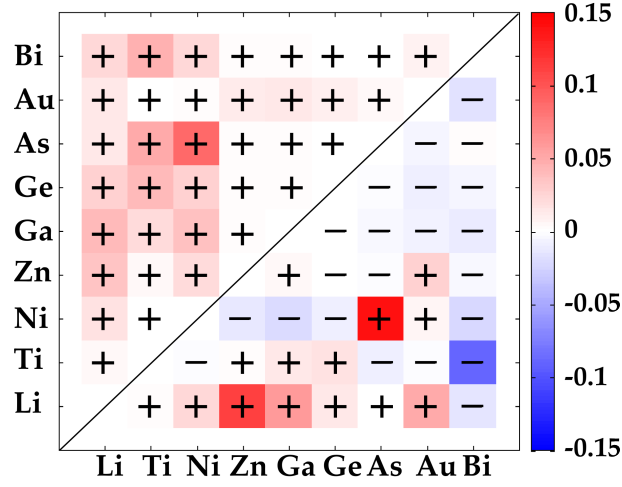


Figure 4.9: Relative deviations from MATTHIESSEN'S rule of the longitudinal resistivity (upper left half) and HALL resistivity (lower right half) for ternary alloys of the form $\text{Cu}(\text{A}_{0.5}\text{B}_{0.5})$.

ANALYSIS OF BEHAVIOUR OF THE CHARGE CONDUCTIVITY, SPIN HALL CONDUCTIVITY AND THE SPIN HALL ANGLE

With the knowledge of the reasonable validity of MATTHIESSEN'S rule, we now can use this rule to investigate the general behaviour of the transport properties, especially the spin HALL angle. This analysis will give insight, whether it is possible to enhance the spin HALL effect in a ternary alloy with respect to the constituent binary alloys. To reduce case-by-case analysis, it is assumed without loss of generality that $\rho_{xx}^{+B} > \rho_{xx}^{+A}$. For further simplification the fact is used that the off-diagonal elements of the spin-dependent conductivity or resistivity tensor are normally much smaller than the diagonal elements. This leads to

$$\sigma_{xx}^{+MR}(w) \approx \frac{1}{\rho_{xx}^{+MR}} = \frac{1}{(1-w)\rho_{xx}^{+A} + w\rho_{xx}^{+B}}, \quad (4.14)$$

$$\sigma_{yx}^{+MR}(w) \approx -\frac{\rho_{yx}^{+MR}}{(\rho_{xx}^{+MR})^2} = -\frac{(1-w)\rho_{yx}^{+A} + w\rho_{yx}^{+B}}{\left((1-w)\rho_{xx}^{+A} + w\rho_{xx}^{+B}\right)^2}, \quad (4.15)$$

where the spin-dependent conductivities are obtained via matrix inversion of the corresponding resistivities. As a result, the charge conductivity is approximated

as the inverse of the longitudinal resistivity, which changes linear with w . Therefore, the functions of the charge conductivities are hyperbolas, which are most pronounced when the ratio of the conductivities $\sigma_{xx}^{+A}/\sigma_{xx}^{+B}$ is large.

The situation for the HALL conductivity is more complicated. Within the used approximations of Eqs. (4.14) and (4.15) $\sigma_{yx}^{+MR}(w)$ has always an extremum, if it is not a constant function. This would suggest an enhancement of the HALL conductivity. However, the extremum might be outside of the physically relevant interval of $w \in [0,1]$, which only provides positive concentrations for both impurities. Furthermore, there always exists a pole of the second order

$$w_p = -\frac{\rho_{xx}^{+A}}{\rho_{xx}^{+B} - \rho_{xx}^{+A}} \quad (4.16)$$

and a zero

$$w_0 = -\frac{\rho_{yx}^{+A}}{\rho_{yx}^{+B} - \rho_{yx}^{+A}} \quad (4.17)$$

of the HALL conductivity, which can occur at an arbitrary value of w . With both quantities the extremum position can be expressed as

$$w_E = 2w_0 - w_p = w_p + 2(w_0 - w_p) . \quad (4.18)$$

These equations are visualized in Fig. 4.10. It shows that the extremum position has the double distance from the pole in comparison to w_0 . To determine whether the extremum is a maximum or a minimum, it helps to investigate the limit at infinity and at the pole:

$$\lim_{w \rightarrow \pm\infty} \sigma_{yx}^{+MR}(w) = \begin{cases} \mp 0 & \text{if } \rho_{yx}^{+B} > \rho_{yx}^{+A} \\ \pm 0 & \text{if } \rho_{yx}^{+B} < \rho_{yx}^{+A} \end{cases} , \quad (4.19)$$

$$\lim_{w \rightarrow \pm w_p} \sigma_{yx}^{+MR}(w) = \begin{cases} -\infty & \text{if } \rho_{yx}^{+MR}(w_p) > 0 \\ \infty & \text{if } \rho_{yx}^{+MR}(w_p) < 0 \end{cases} . \quad (4.20)$$

These conditions by themselves cannot determine the type of extremum. However, with the Eqs. (4.14)-(4.20) a construction as in Fig. 4.10 can be done easily to clarify the behaviour of the spin HALL conductivity.

To obtain pronounced extrema it is necessary that w_0 and w_p are close to each other

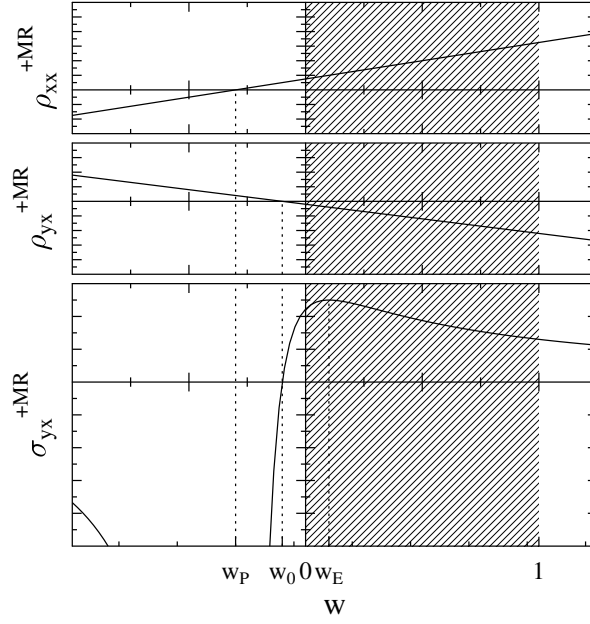


Figure 4.10: Resistivities for spin-up channel and spin HALL conductivity for a model system in arbitrary units. The physically relevant interval $w \in [0, 1]$ is shaded in gray.

as well as to zero, since this assures a rapid change of the function. Consequently, an important condition is $\rho_{xx}^B \gg \rho_{xx}^A$.

An interesting point is to investigate, whether a possible enhancement of the spin HALL conductivity can increase the efficiency of the spin HALL effect. Therefore, the spin HALL angle

$$\alpha(w) = \frac{\sigma_{yx}^{+MR}}{\sigma_{xx}^{+MR}} = -\frac{(1-w)\rho_{yx}^{+A} + w\rho_{yx}^{+B}}{(1-w)\rho_{xx}^{+A} + w\rho_{xx}^{+B}} \quad (4.21)$$

was tested for an extremum with respect to w . One obtains $\alpha^A = -\rho_{yx}^{+A}/\rho_{xx}^{+A} = -\rho_{yx}^{+B}/\rho_{xx}^{+B} = \alpha^B$. However, this leads only to the trivial solution of a constant spin HALL angle for the ternary alloy. In other words a ratio of two quantities depending linearly on the same parameter can not have an extremum. This indicates that the efficiency of the spin HALL effect in a ternary alloy can not be amplified.

4.4 SPIN HALL & SPIN NERNST EFFECT IN TERNARY ALLOYS

In this section transport properties related to the spin HALL effect and spin NERNST effect in ternary alloys are investigated [78]. It is of special interest, whether the efficiencies of both effects can be enhanced in a ternary alloy with respect to the constituent binary alloys of equal total impurity concentration. This knowledge allows the tailoring of materials to obtain increased spin currents. The results from MATTHIESSEN'S rule are provided in the whole range of the impurity weighting factor w . Additionally, some values are given for the full calculations, where the linearized BOLTZMANN equation was solved with a microscopic transition probability of the ternary alloy, according to Eq. (3.145). For the presentation of the results three ternary alloys of the form $\text{Cu}(\text{A}_{1-w}\text{B}_w)$ were chosen, which show distinct characteristics.

4.4.1 SPIN HALL EFFECT

In Fig. 4.11 the spin HALL conductivity and the charge conductivity are presented for $\text{Cu}(\text{Zn}_{1-w}\text{Ti}_w)$, $\text{Cu}(\text{Bi}_{1-w}\text{Ti}_w)$, and $\text{Cu}(\text{Au}_{1-w}\text{Bi}_w)$ dilute alloys, which describe the induced charge and spin current density in response to an electric field, respectively. In addition, the corresponding spin HALL angle is shown, which represents the efficiency of the phenomenon. First of all, this figure confirms the good agreement between MATTHIESSEN'S rule (lines) and the full calculations (dots). The charge conductivity, presented in the mid panel, shows a similar qualitative behaviour for all three alloys. The corresponding curves are hyperbolas, whose curvature increases with the ratio $\sigma_{xx}^A/\sigma_{xx}^B$. In contrast to that, the spin HALL conductivities in the upper panel have three distinct features. Whereas the spin HALL conductivity of the $\text{Cu}(\text{Bi}_{1-w}\text{Ti}_w)$ alloy is also hyperbola-like, the curves for the other two alloys have an extremum. However, in the case of the $\text{Cu}(\text{Zn}_{1-w}\text{Ti}_w)$ alloy this does not lead to a real enhancement of the effect. Since the corresponding spin HALL conductivities of the two constituent binary alloys have opposite signs, the extremum has not the global absolute value, which is instead adopted by the $\text{Cu}(\text{Zn})$ alloy. The most interesting behaviour has the $\text{Cu}(\text{Au}_{1-w}\text{Bi}_w)$ alloy. Although the spin HALL conductivities of the related binary alloys have approximately the same value, this quantity shows a strong enhancement by a factor of about three for the $\text{Cu}(\text{Au}_{0.9}\text{Bi}_{0.1})$ alloy. Similar to the $\text{Cu}(\text{Zn}_{1-w}\text{Ti}_w)$ alloy, the enhancement is caused by the strong decay of the longitudinal conductivity, which

enters when the HALL resistivity

$$\rho_{yx}^+ = -\frac{\sigma_{yx}^+}{(\sigma_{xx}^+)^2 + (\sigma_{yx}^+)^2} \quad (4.22)$$

is calculated. However, now the extremum has a global absolute value and therefore the spin HALL conductivity is really increased. Nevertheless, if one discusses the results for the spin HALL angle, shown in the lower panel of Fig. 4.11, the expected scenario from the analysis of MATTHIESSEN'S rule is obtained. Namely, the spin HALL angle of a ternary alloy stays always between those of the constituent binary alloys. Therefore, the efficiency of the spin HALL effect is not enhanced for the ternary alloys, which is additionally confirmed by the full ab initio calculations.

4.4.2 SPIN NERNST EFFECT

For the spin NERNST effect the quantities, which provide the heat and spin current density in linear response to a temperature gradient, are presented in Fig. 4.12. They are the heat conductivity and the spin NERNST conductivity, respectively. In addition, the ratio of both, which describes the efficiency of the heat to spin current conversion, is shown. The heat conductivity in the mid panel has the same behaviour as the charge conductivity in Fig. 4.11, which is a consequence of the WIEDEMANN-FRANZ law given by Eq. (3.105). In the case of the spin NERNST conductivity, shown in the top panel, extrema are received for all three curves. However, only for the $\text{Cu}(\text{Bi}_{1-w}\text{Ti}_w)$ alloy there is a global extremum being larger than the related values of the constituent binary alloys. Obviously, this extremum is not only provided by L_{0yx}^+ in Eq. (4.6), which is proportional to the spin HALL conductivity. If this quantity would be the dominating contribution, then the behaviour of the spin NERNST and spin HALL conductivity in the Figs. 4.12 and 4.11 should be similar. Furthermore, with $\sigma_{xx} \propto \kappa$ one would have practically the same correlation as between the longitudinal and HALL conductivity of the spin HALL effect. Therefore an extremum would be impossible for the efficiency. However, in contrast to the spin HALL angle, the efficiency of the spin NERNST effect, shown in the lower panel of Fig. 4.12, can have an extremum. Namely, the efficiency of the $\text{Cu}(\text{Bi}_{0.75}\text{Ti}_{0.25})$ alloy shows an enhancement of about 4.5 in comparison to the binary alloy $\text{Cu}(\text{Bi})$. This is possible because the spin NERNST conductivity depends on different linear transport coefficients, where the energy enters via zero and first

order in Eq. (3.95). As a result, the spin NERNST conductivity is influenced by the longitudinal and HALL conductivity itself and by their corresponding derivatives at the FERMI energy. Due to the complex nature of the spin NERNST conductivity and absence of its clear correlation with the heat conductivity, an extremum is not prohibited for the efficiency generally. Actually, a pronounced extremum occurs for the $\text{Cu}(\text{Bi}_{1-w}\text{Ti}_w)$ alloy.

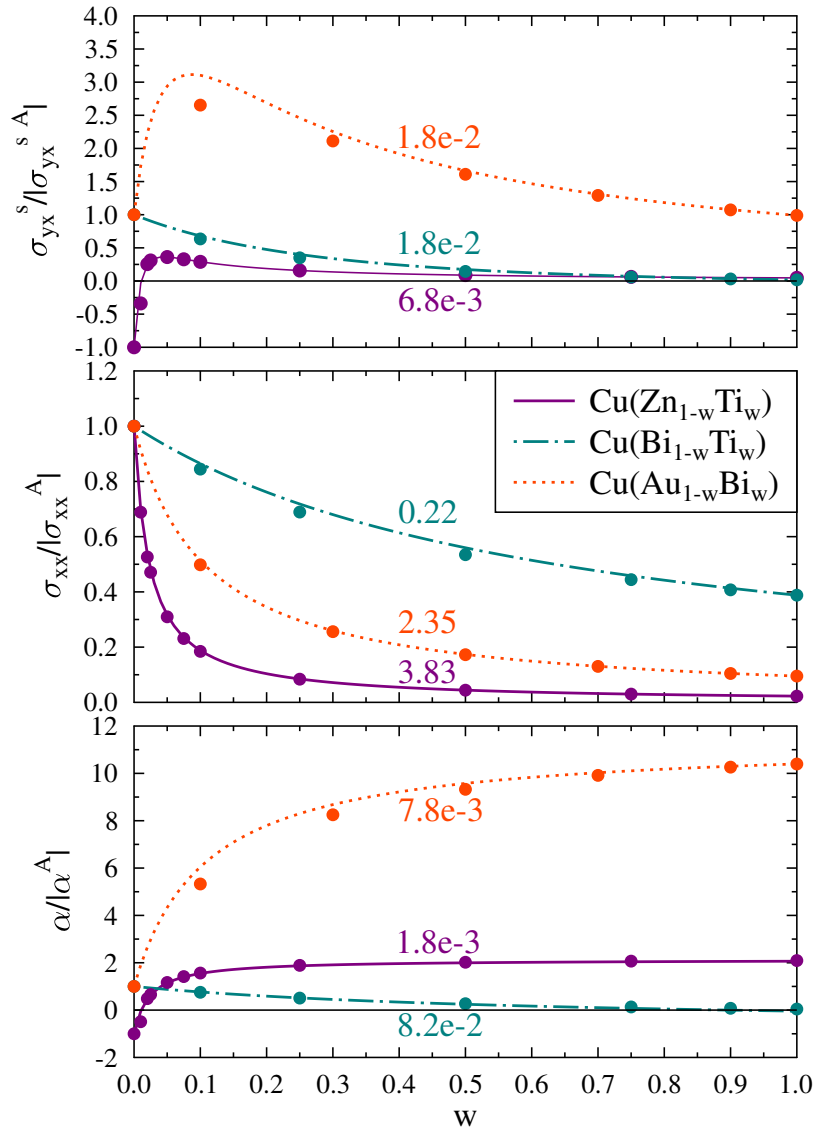


Figure 4.11: Spin HALL conductivity, longitudinal conductivity, and spin HALL angle for three $\text{Cu}(\text{A}_{1-w}\text{B}_w)$ alloys. An approximation via MATTHIESSEN'S rule (lines) and the values obtained with full calculations (dots) are shown. All curves are normalized to have the absolute values for $\text{Cu}(\text{A})$ alloy equal to one. The multiplication of the curves with the scaling factors provides the actual values of the conductivities in units of $(\mu\Omega\text{cm})^{-1}$ and α (dimensionless).

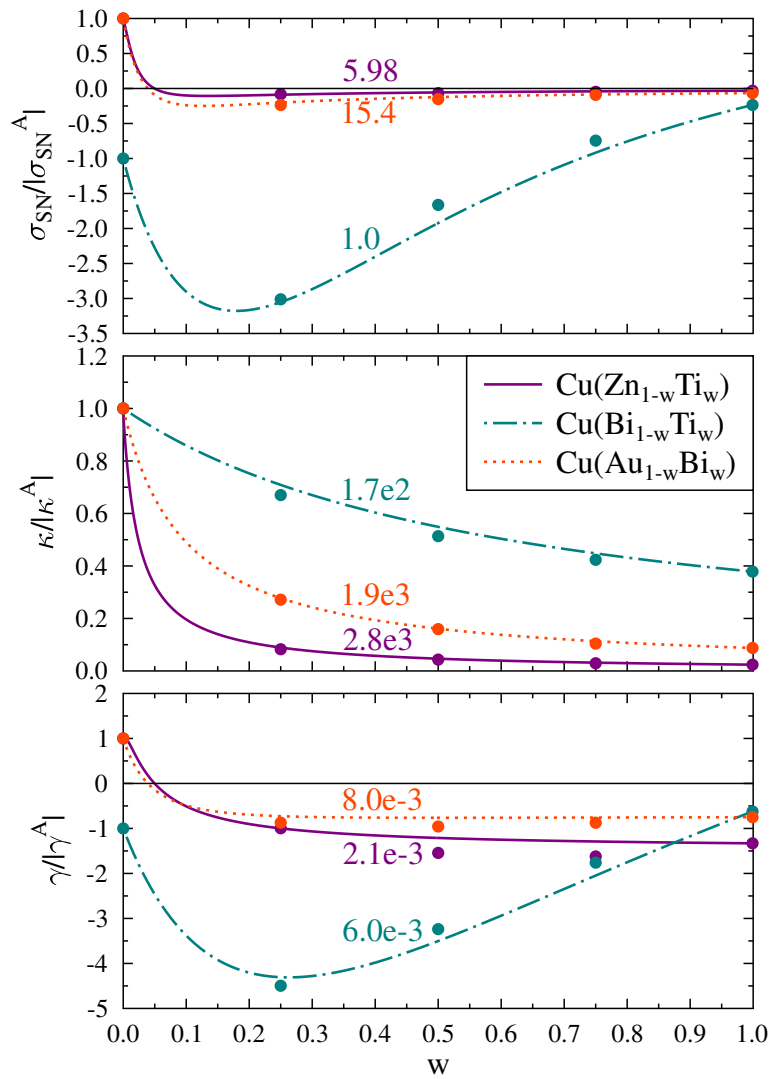


Figure 4.12: Spin NERNST conductivity, heat conductivity and the ratio of both calculated via MATTHIESSEN'S rule (lines) and full calculations (dots) at 300 K for three $\text{Cu}(\text{A}_{1-w}\text{B}_w)$ alloys. The given factors provide σ_{SN} in A/Km , κ in W/Km , and γ in $1/\text{V}$.

5 SUMMARY

In this work two transverse spin transport phenomena, the spin HALL effect and the spin NERNST effect, were investigated by means of *ab initio* calculations. These phenomena refer to the generation of a spin current/spin accumulation transverse to an applied electric field or temperature gradient, respectively. Both effects occur in non-magnetic systems and are caused by spin-orbit interaction. Particularly, the extrinsic skew-scattering mechanism was considered, which is the dominant contribution in dilute alloys. It contributes via asymmetric scattering at substitutional impurities.

For calculations of the electronic structure a relativistic KORRINGA-KOHN-ROSTOKER method was used. The GREEN functions of the host and of the defect system were obtained self-consistently. From the elements of the transition matrix the microscopic transition probabilities describing the scattering processes were calculated.

To obtain the transport properties a linearized BOLTZMANN equation was solved. At this point, it was essential to include the so-called scattering-in term, which is responsible for the considered transverse spin transport. For the description of the spin NERNST effect, a numerical integration over an energy range had to be performed. For this purpose I wrote a program, which calculates the presented transport properties from an energy-dependent conductivity tensor. Furthermore, I developed the necessary formulas for the theoretical description of the spin NERNST effect.

The mentioned methods were first applied to calculate the spin NERNST effect in Cu-based dilute alloys with only one type of impurity. It is shown that the sign and the size of the phenomenon depends strongly on the impurity type. Furthermore, it is demonstrated that with the spin NERNST effect one can create spin currents of the same order of magnitude as via the spin HALL effect. For this purpose it is necessary to have very large temperature gradients of the order of $10 \text{ K}/\mu\text{m}$,

which can be attained in practice with laser pulses [74]. On the other hand, this implies that the spin NERNST effect causes only tiny additional spin currents or spin accumulations, when an accidental temperature gradient is present during spin HALL experiments.

In addition, the two considered phenomena were investigated in Cu-based ternary alloys. Apart from full calculations for some of the considered alloys of the general form $\text{Cu}(\text{A}_{1-w}\text{B}_w)$, MATTHIESSEN'S rule was used to obtain the transport properties in the whole range of the impurity weighting factor w . For this purpose I developed the formalism, how this rule can be applied not only to the charge conductivity but also to the spin HALL conductivity in the relativistic case. Still, only the transport properties of the related binary alloys are required. For the considered alloys with equal amount of two impurities, $\text{Cu}(\text{A}_{0.5}\text{B}_{0.5})$, it was found that the relative deviations of the fully calculated resistivities from MATTHIESSEN'S rule are less than 15%. This proves that MATTHIESSEN'S rule offers a good approximation, which can be used for a simple estimation of the transport properties for the ternary alloys. Furthermore, the sign of these deviations was analyzed. In contrast to the longitudinal resistivity, where the deviations are always positive, both signs were found for the off-diagonal elements of the spin-dependent resistivity tensor. A further aim was to show, how the efficiency of the spin HALL and spin NERNST effect can be enhanced in ternary alloys with respect to the constituent binary alloys. This is done by an appropriate weighting of the two impurity types keeping the total impurity concentration constant. As shown, it is possible to enhance the spin HALL conductivity, but not the spin HALL angle, the efficiency of the charge to spin current conversion for the spin HALL effect. This implies that the efficiency of this phenomenon in dilute alloys with several types of impurities can never be larger than the one of the binary alloy with the highest spin HALL angle among the present impurities. The reason for this is nicely explained within the approximation of MATTHIESSEN'S rule, where the spin HALL angle is written as a ratio of two functions linearly depending on the impurity weighting factor. An enhancement in comparison to the binary alloys is therefore impossible, since the function can not have an extremum due to trivial mathematical reasons.

By contrast, for the spin NERNST effect not only the spin NERNST conductivity, but also the efficiency of this phenomenon can be increased. Namely, an enhancement up to a factor of 4.5 was found. This result in combination with MATTHIESSEN'S rule offers a way to design materials with efficient spin current generation by temperature gradients in ternary alloys.

LIST OF SYMBOLS

LATIN

\mathbf{B}	magnetic field
\mathbf{B}^{eff}	effective magnetic field
c	speed of light
C	CLEBSCH-GORDON coefficients
e	elementary charge, EULER's number
\mathbf{E}	electric field
\mathcal{E}	energy, energy functional
\mathcal{E}_F	FERMI energy
\mathcal{E}_k	energy dispersion
\mathcal{E}_0	ground state energy
\mathcal{E}_{xc}	exchange-correlation energy
$\mathcal{E}_{xc}^{\text{LDA}}$	exchange-correlation energy in local density approximation
f_k	distribution function
f_k^0	FERMI function
$f_{QQ'}, g_{QQ'}$	radial parts of the relativistic regular solutions for a single-site scatterer
g_k	deviation from equilibrium distribution function
G, \mathring{G}	GREEN functions
G^+	retarded GREEN function
G^-	advanced GREEN function
$G_{LL'}^{nn'}, G_{QQ'}^{nn'}, G_{QQ'}^{nn'\mu\mu'}$	structure constants
H, \mathring{H}	Hamilton operators
\hbar	reduced Planck constant
i	imaginary unit
\Im	imaginary part
j	quantum number of total angular momentum
\mathbf{j}	charge current density
\mathbf{j}^s	spin current density
\mathbf{J}	operator of total angular momentum
J_z	operator of the z projection of the total angular momentum
k	$\{\mathbf{k}, \nu\}$
\mathbf{k}	wave vector
k_B	BOLTZMANN constant
K	operator of the relativistic angular momentum
\mathbf{K}_k	generalized force

l	quantum number of angular momentum
L	$\{l, m\}$
\hat{L}_n	general transport coefficients
m	rest mass of electron, magnetic quantum number
\mathbf{m}	magnetization density
M	KKR-matrix
n	electron density
n_0	ground state electron density
N	number of atoms
N_e	number of electrons
\mathbf{p}	momentum
$P_{kk'}$	microscopic transition probability
PV	CAUCHY principal value
\mathbf{q}	heat current density
\overline{Q}	$\{\kappa, \mu_j\}$
\underline{Q}	$\{-\kappa, \mu_j\}$
\mathbf{r}	place
R_{MT}^n	muffin-tin radius
$R_{ASA}^{n\mu}$	radius of atomic sphere approximation
R_L^n	non-relativistic regular solutions for the single-site scatterer
R_l^n	radial part of the non-relativistic regular solutions for the single-site scatterer
R_Q	relativistic regular solutions for the single-site scatterer
\mathbf{R}^n	vector to center of cell n
s_k^z	spin expectation value in z direction
\hat{S}	thermopower (SEEBECK coefficient)
\hat{S}^s	spin SEEBECK coefficient
S_k	FERMI surface
t	time
t_Q^n	single site t-matrix or difference of two of them
T	temperature, T operator
T_e, T_c	kinetic energy for electrons and nuclei
$T_{kk'}$	transition matrix elements
Tr	Trace
U	voltage
\mathbf{v}_a	anomalous velocity
\mathbf{v}_k	group velocity
V	system volume
V, \hat{V}	potential
V_{BZ}	volume of the BRIOULLIN zone
V^{eff}	effective potential
V_{ee}, V_{ec}, V_{cc}	COULOMB interaction between electrons and nuclei
V^n	cell-centered potential or difference of two potentials
w	weighting factor between two types of impurities

X	left hand side of BOLTZMANN equation
Y_L	spherical harmonics
GREEK	
α	spin HALL angle
$\hat{\alpha}, \hat{\alpha}_i$	$\begin{pmatrix} 0 & \hat{\sigma} \\ \hat{\sigma} & 0 \end{pmatrix}, \begin{pmatrix} 0 & \hat{\sigma}_i \\ \hat{\sigma}_i & 0 \end{pmatrix}$
$\hat{\beta}$	$\begin{pmatrix} \mathbb{1}_2 & 0 \\ 0 & -\mathbb{1}_2 \end{pmatrix}$
γ	efficiency of the spin NERNST effect
δ	delta function, KRONECKER delta, variation
$\varepsilon_i, \hat{\varepsilon}_i$	eigenenergies
$\varepsilon_{xc}^{\text{hom}}$	exchange-correlation energy of an homogeneous non-interacting electron gas
η	imaginary part of z
κ	quantum number of the relativistic angular momentum
$\hat{\kappa}$	heat conductivity
Λ_k	mean free path
μ	chemical potential, index of the basis atoms
μ_j	relativistic magnetic quantum number
ν	band index
π	pi
$\hat{\rho}$	resistivity
$\hat{\sigma}$	charge conductivity
$\hat{\sigma}, \hat{\sigma}_i$	PAULI spin matrices
$\hat{\sigma}^s$	spin conductivity
$\hat{\sigma}_{SN}$	spin NERNST conductivity
$\hat{\Sigma}, \hat{\Sigma}_i$	$\begin{pmatrix} \hat{\sigma} & 0 \\ 0 & \hat{\sigma} \end{pmatrix}, \begin{pmatrix} \hat{\sigma}_i & 0 \\ 0 & \hat{\sigma}_i \end{pmatrix}$
τ_k	relaxation time
Φ	trial function
Φ_s	spinor basis functions
χ_Q	spin spherical harmonics
$\Psi, \psi, \psi_i, \hat{\psi}_i$	wave functions
Ω_k	BERRY curvature
OTHER SYMBOLS	
$\mathbb{1}$	unit operator
$\mathbb{1}_n$	unit matrix of dimension $n \times n$
∇	nabla operator
\circ	tensor product
$*$	conjugate complex
\dagger	adjoint
\times	conjugate complex for radial part only

BIBLIOGRAPHY

- [1] S. A. Wolf, D. D. Awschalom, R. A. Buhrman, J. M. Daughton, S. von Molnár, M. L. Roukes, A. Y. Chtchelkanova, and D. M. Treger, "Spintronics: a spin-based electronics vision for the future," *Science*, vol. 294, pp. 1488–1495, Nov. 2001.
- [2] G. A. Prinz, "Magnetoelectronics," *Science*, vol. 282, pp. 1660–1663, Nov. 1998.
- [3] O. Stern and W. Gerlach, "Das magnetische Moment des Silberatoms.," *Zeitschrift für Physik*, vol. 9, pp. 353–355, 1922.
- [4] S. S. P. Parkin, M. Hayashi, and L. Thomas, "Magnetic domain-wall racetrack memory," *Science*, vol. 320, pp. 190–194, Apr. 2008.
- [5] P. Sharma, "How to Create a Spin Current," *Science*, vol. 307, pp. 531–533, Jan. 2005.
- [6] M. N. Baibich, J. M. Broto, A. Fert, F. Nguyen Van Dau, and F. Petroff, "Giant Magnetoresistance of (001)Fe/(001)Cr Magnetic Superlattices," *Phys. Rev. Lett.*, vol. 61, no. 21, pp. 2472–2475, 1988.
- [7] G. Binasch, P. Grünberg, F. Saurenbach, and W. Zinn, "Enhanced magnetoresistance in layered magnetic structures," *Phys. Rev. B*, vol. 39, no. 7, pp. 4828–4830, 1989.
- [8] "<http://www.nobelprize.org>," 2007.
- [9] "<http://www.research.ibm.com/research/gmr.html>," 2013.
- [10] M. Julliere, "Tunneling between ferromagnetic films," *Phys. Lett.*, vol. 54A, no. 3, pp. 225–226, 1975.

- [11] T. Kimura, Y. Otani, T. Sato, S. Takahashi, and S. Maekawa, "Room-Temperature Reversible Spin Hall Effect," *Phys. Rev. Lett.*, vol. 98, p. 156601, Apr. 2007.
- [12] M. Gradhand, D. V. Fedorov, P. Zahn, and I. Mertig, "Extrinsic Spin Hall Effect from First Principles," *Phys. Rev. Lett.*, vol. 104, p. 186403, May 2010.
- [13] M. Gradhand, D. V. Fedorov, P. Zahn, and I. Mertig, "Skew Scattering Mechanism by an Ab Initio Approach: Extrinsic Spin Hall Effect in Noble Metals," *Solid State Phenom.*, vol. 168-169, pp. 27–30, Dec. 2011.
- [14] M. Gradhand, *The Extrinsic Spin Hall Effect*. PhD thesis, Martin-Luther-Universität Halle-Wittenberg, 2010.
- [15] G. E. W. Bauer, A. H. MacDonald, and S. Maekawa, "Spin Caloritronics," *Solid State Commun.*, vol. 150, pp. 459–460, Mar. 2010.
- [16] G. E. W. Bauer, E. Saitoh, and B. J. van Wees, "spin caloritronics," *Nature Mater.*, vol. 11, p. 391, 2012.
- [17] M. Johnson and R. H. Silsbee, "Thermodynamic analysis of interfacial transport and of the thermomagnetolectric system," *Phys. Rev. B*, vol. 35, no. 10, pp. 4959–4972, 1987.
- [18] K. Uchida, S. Takahashi, K. Harii, J. Ieda, W. Koshibae, K. Ando, S. Maekawa, and E. Saitoh, "Observation of the spin Seebeck effect.," *Nature*, vol. 455, pp. 778–781, Oct. 2008.
- [19] K. Uchida, S. Takahashi, J. Ieda, K. Harii, K. Ikeda, W. Koshibae, S. Maekawa, and E. Saitoh, "Phenomenological analysis for spin-Seebeck effect in metallic magnets," *J. Appl. Phys.*, vol. 105, no. 7, p. 07C908, 2009.
- [20] K. Uchida, J. Xiao, H. Adachi, J. Ohe, S. Takahashi, J. Ieda, T. Ota, Y. Kajiwara, H. Umezawa, H. Kawai, G. E. W. Bauer, S. Maekawa, and E. Saitoh, "Spin Seebeck insulator," *Nature Mater.*, vol. 9, pp. 894–897, Sept. 2010.
- [21] C. M. Jaworski, J. Yang, S. Mack, D. D. Awschalom, J. P. Heremans, and R. C. Myers, "Observation of the spin-Seebeck effect in a ferromagnetic semiconductor," *Nature Mater.*, vol. 9, pp. 898–903, Sept. 2010.

- [22] J. Xiao, G. E. W. Bauer, K. Uchida, E. Saitoh, and S. Maekawa, "Theory of magnon-driven spin Seebeck effect," *Phys. Rev. B*, vol. 81, p. 214418, June 2010.
- [23] A. Slachter, F. L. Bakker, J.-P. Adam, and B. J. van Wees, "Thermally driven spin injection from a ferromagnet into a non-magnetic metal," *Nature Phys.*, vol. 6, pp. 879–882, 2010.
- [24] I. Mertig, R. Zeller, and P. H. Dederichs, "Ab initio calculations of the deviations from Matthiesen's rule for dilute ternary alloys," *Phys. Rev. B*, vol. 49, no. 17, pp. 767–772, 1994.
- [25] A. Matthiessen and C. Vogt, "On the influence of temperature on the electric conductive-power of alloys," *Philos. T. R. Soc. Lond.*, vol. 154, p. 167, 1864.
- [26] Y. K. Kato, R. C. Myers, A. C. Gossard, and D. D. Awschalom, "Observation of the Spin Hall Effect in Semiconductors," *Science*, vol. 306, pp. 1910–1913, 2004.
- [27] N. Nagaosa, J. Sinova, S. Onoda, A. H. MacDonald, and N. P. Ong, "Anomalous Hall effect," *Rev. Mod. Phys.*, vol. 82, pp. 1539–1592, May 2010.
- [28] R. Karplus and J. Luttinger, "Hall Effect in Ferromagnetics," *Phys. Rev.*, vol. 95, no. 5, pp. 1154–1160, 1954.
- [29] T. Jungwirth, Q. Niu, and A. MacDonald, "Anomalous Hall Effect in Ferromagnetic Semiconductors," *Phys. Rev. Lett.*, vol. 88, p. 207208, May 2002.
- [30] M. Onoda and N. Nagaosa, "Topological Nature of Anomalous Hall Effect in Ferromagnets," *J. Phys. Soc. Jpn.*, vol. 71, p. 19, 2002.
- [31] M. Chang and Q. Niu, "Berry phase, hyperorbits, and the Hofstadter spectrum: Semiclassical dynamics in magnetic Bloch bands," *Phys. Rev. B*, vol. 53, pp. 7010–7023, Mar. 1996.
- [32] G. Sundaram and Q. Niu, "Wave-packet dynamics in slowly perturbed crystals: Gradient corrections and Berry-phase effects," *Phys. Rev. B*, vol. 59, no. 23, pp. 14915–14925, 1999.

- [33] M. Berry, "Quantal phase factors accompanying adiabatic changes," *Proc. R. Soc. Lond. A*, vol. 392, pp. 45–57, 1984.
- [34] Y. Yao, L. Kleinman, A. MacDonald, J. Sinova, T. Jungwirth, D.-s. Wang, E. Wang, and Q. Niu, "First Principles Calculation of Anomalous Hall Conductivity in Ferromagnetic bcc Fe," *Phys. Rev. Lett.*, vol. 92, p. 037204, Jan. 2004.
- [35] G. Y. Guo, S. Murakami, T.-W. Chen, and N. Nagaosa, "Intrinsic Spin Hall Effect in Platinum: First-Principles Calculations," *Phys. Rev. Lett.*, vol. 100, p. 096401, Mar. 2008.
- [36] J. Smit, "The spontaneous Hall effect in ferromagnetics I," *Physica*, vol. 21, pp. 877–887, 1955.
- [37] J. Smit, "The spontaneous Hall effect in ferromagnetics II," *Physica*, vol. 24, pp. 39–51, 1958.
- [38] L. Berger, "Influence of spin-orbit interaction on the transport processes in ferromagnetic nickel alloys, in the presence of a degeneracy of the 3d band," *Physica*, vol. 30, pp. 1141–1159, June 1964.
- [39] L. Berger, "Side-Jump Mechanism for the Hall Effect of Ferromagnets," *Phys. Rev. B*, vol. 2, p. 4559, 1970.
- [40] M. Born and R. Oppenheimer, "Zur Quantentheorie der Molekeln," *Annalen der Physik*, vol. 84, no. 20, pp. 457–484, 1927.
- [41] P. Hohenberg and W. Kohn, "Inhomogeneous Electron Gas," *Phys. Rev.*, vol. 136, no. 3B, pp. 864–871, 1964.
- [42] W. Kohn and L. J. Sham, "Self-Consistent Equations Including Exchange and Correlation Effects," *Phys. Rev.*, vol. 140, no. 4A, pp. 1133–1138, 1965.
- [43] J. Korrynga, "On the calculation of the energy of a Bloch wave in a metal," *Physica*, vol. 13, no. 6-7, pp. 392–400, 1947.
- [44] W. Kohn and N. Rostoker, "Solution of the Schrödinger Equation in Periodic Lattices with an Application to Metallic Lithium," *Phys. Rev.*, vol. 94, no. 5, pp. 1111–1120, 1954.

- [45] R. Zeller, P. H. Dederichs, B. Úfalussy, L. Szunyogh, and P. Weinberger, "Theory and convergence properties of the screened Korringa-Kohn-Rostoker method," *Phys. Rev. B*, vol. 52, no. 12, pp. 8807–8812, 1995.
- [46] P. Zahn, *Screened Korringa-Kohn-Rostoker-Methode für Vielfachschichten*. PhD thesis, Technische Universität Dresden, 1998.
- [47] J. Binder, *Giant Magnetoresistance, eine ab-initio Beschreibung*. PhD thesis, Technische Universität Dresden, 2000.
- [48] I. Mertig, E. Mrosan, and P. Ziesche, *Multiple Scattering Theory of Point Defects in Metals: Electronic Properties*. Leipzig: Teubner-Verlag, 1987.
- [49] S. Takada, "Relativistic Formulation of the Green's Function Method in Periodic Lattices," *Prog. Theor. Phys.*, vol. 36, no. 2, pp. 224–236, 1966.
- [50] P. Strange, J. Staunton, and B. L. Gyorffy, "Relativistic spin-polarised scattering theory - solution of the single-site problem," *J. Phys. C: Solid State Phys.*, vol. 17, pp. 3355–3371, 1984.
- [51] P. Strange, H. Ebert, J. B. Staunton, and B. L. Gyorffy, "A relativistic spin-polarised multiple-scattering theory , with applications to the calculation of the electronic structure of condensed matter," *J. Phys.: Condens. Matter*, vol. 1, pp. 2959–2975, 1989.
- [52] L. Szunyogh, B. Úfalussy, and P. Weinberger, "Magnetic anisotropy of iron multilayers on Au(001): First-principles calculations in terms of the fully relativistic spin-polarized screened KKR method," *Phys. Rev. B*, vol. 51, no. 15, pp. 9552–9559, 1995.
- [53] M. Czerner, *Beiträge zur Theorie des Elektronentransports in Systemen mit nichtkollinearer magnetischer Ordnung*. PhD thesis, Martin-Luther-Universität Halle-Wittenberg, 2009.
- [54] J. Zabloudil, R. Hammerling, L. Szunyogh, and P. Weinberger, *Electron Scattering in Solid Matter*. Berlin: Springer Verlag, 2005.
- [55] J. Zabloudil, R. Hammerling, L. Szunyogh, and P. Weinberger, "Bulk and surface properties of metals by full-charge-density screened Korringa-Kohn-Rostoker calculations," *Phys. Rev. B*, vol. 73, p. 115410, Mar. 2006.

- [56] M. Gradhand, D. V. Fedorov, P. Zahn, and I. Mertig, "Fully relativistic ab initio treatment of spin-flip scattering caused by impurities," *Phys. Rev. B*, vol. 81, p. 020403, Jan. 2010.
- [57] N. Papanikolaou, R. Zeller, and P. H. Dederichs, "Conceptual improvements of the KKR method," *J. Phys.: Condens. Matter*, vol. 14, pp. 2799–2823, 2002.
- [58] P. Zahn, *Transport phenomena in metallic nanostructures : An ab initio approach*. PhD thesis, Technische Universität Dresden, 2003.
- [59] I. Mertig, "Transport properties of dilute alloys," *Rep. Prog. Phys.*, vol. 62, pp. 237–276, Sept. 1999.
- [60] P. Strange, *Relativistic Quantum Mechanics*. Cambridge University Press, 1998.
- [61] H. A. Kramers, "Théorie générale de la rotation paramagnétique dans les cristaux," *Proc. Acad. Sci. Amsterdam*, vol. 33, pp. 959–972, 1930.
- [62] R. J. Elliott, "Theory of the Effect of Spin-Orbit Coupling on Magnetic Resonance in Some Semiconductors," *Phys. Rev.*, vol. 96, no. 2, pp. 266–279, 1954.
- [63] F. Pientka, M. Gradhand, D. V. Fedorov, I. Mertig, and B. L. Györfy, "Gauge freedom for degenerate Bloch states," *Phys. Rev. B*, vol. 86, p. 054413, Aug. 2012.
- [64] M. Gradhand, M. Czerner, D. V. Fedorov, P. Zahn, B. Y. Yavorsky, L. Szunyogh, and I. Mertig, "Spin polarization on Fermi surfaces of metals by the KKR method," *Phys. Rev. B*, vol. 80, p. 224413, Dec. 2009.
- [65] E. Merzbacher, *Quantum Mechanics*. New York: Wiley, 1970.
- [66] Y. Yafet, *Solid State Physics*. New York: Academic Press, 1963.
- [67] W. Kohn and J. Luttinger, "Quantum Theory of Electrical Transport Phenomena," *Phys. Rev.*, vol. 108, no. 3, p. 590, 1957.
- [68] J. Luttinger and W. Kohn, "Quantum Theory of Electrical Transport Phenomena. II," *Phys. Rev.*, vol. 109, no. 6, p. 1892, 1958.
- [69] J. Ziman, *Principles of the Theory of Solids*. Cambridge: Cambridge University Press, 1964.

- [70] G. Wiedemann and R. Franz, "Ueber die Wärme-Leitungsfähigkeit der Metalle," *Annalen der Physik und Chemie*, vol. 165, no. 8, p. 497, 1853.
- [71] K. Tauber, M. Gradhand, D. V. Fedorov, and I. Mertig, "Extrinsic Spin Nernst Effect from First Principles," *Phys. Rev. Lett.*, vol. 109, p. 026601, July 2012.
- [72] Z. Ma, "Spin Hall effect generated by a temperature gradient and heat current in a two-dimensional electron gas," *Solid State Commun.*, vol. 150, pp. 510–513, Mar. 2010.
- [73] J. Ziman, *Electrons and Phonons*. Oxford: Oxford University Press, 2001.
- [74] M. Weiler, M. Althammer, F. D. Czeschka, H. Huebl, M. S. Wagner, M. Opel, I.-M. Imort, G. Reiss, A. Thomas, R. Gross, and S. T. B. Goennenwein, "Local Charge and Spin Currents in Magnetothermal Landscapes," *Phys. Rev. Lett.*, vol. 108, p. 106602, Mar. 2012.
- [75] T. Yang, T. Kimura, and Y. Otani, "Giant spin-accumulation signal and pure spin-current-induced reversible magnetization switching," *Nat. Phys.*, vol. 4, pp. 851–854, Oct. 2008.
- [76] S. Wimmer, D. Ködderitzsch, K. Chadova, and H. Ebert, "First-principles linear response description of the spin Nernst effect," *Phys. Rev. B*, vol. 88, p. 201108, Nov. 2013.
- [77] J. Bass, *Electrical Resistivity of Pure Metals and Alloys*. Landolt-Börnstein New Series, Group III, Part (a), vol. 15, New York: Springer, 1982.
- [78] K. Tauber, D. V. Fedorov, M. Gradhand, and I. Mertig, "Spin Hall and spin Nernst effect in dilute ternary alloys," *Phys. Rev. B*, vol. 87, p. 161114(R), Apr. 2013.

PUBLICATIONS

Katarina Tauber, Martin Gradhand, Dmitry V. Fedorov, and Ingrid Mertig. *Extrinsic Spin Nernst Effect from First Principles*. PRL **109**, 026601 (2012).

Katarina Tauber, Dmitry V. Fedorov, Martin Gradhand, and Ingrid Mertig. *Spin Hall and Spin Nernst Effect in Dilute Ternary Alloys*, PRB **87**, 161114(R) (2013).

ACKNOWLEDGEMENT

It is not important to achieve a goal, but what you learn on your way. Therefore, huge thanks go first and foremost to the indispensable troika - Ingrid, Dima, and Martin -, who accompanied me on the challenging path of becoming a physicist. I could always rely on their distinct talents, which helped immensely improving my work.

I thank Ingrid for providing me a place to grow, while allowing me to be myself and accepting my needs. Furthermore, she always found research topics, which suited me. Finally, I am really grateful, that she still believed in my abilities, when I could not.

I thank Dima for many fruitful discussions with his talent to explain complicated things in a comprehensible way. He also always did a good job as editor and missed no opportunity to cheer me up. Most importantly, he gave me the best possible advice, when I needed it most.

I thank Martin for supervising my first steps into research. With his introduction to our KKR code he provided me the basis of my work. Due to his always available broad knowledge he could often express really helpful criticism. His sometimes provoking questions encouraged me to think deeper.

Apart from that, I am grateful to many other people. However, I will not mention further names, because I don't want to leave anyone out. Namely, sometimes even a very subtle action or comment can have a huge impact. Special thanks go of course to my colleagues, who always shared a lot of interesting, funny, shocking and inspiring information. This usually made lunchtime and group events a bliss. Furthermore, I want to thank everyone, who helped me during this tough last year to regain my physical and particular mental strength, which was so desperately needed to finish this work.

Last but not least, I am really thankful for my family, which was supportive in so many ways...

CURRICULUM VITAE

Personal data:

name: Katarina Tauber
address: Burgstraße 48, 06114 Halle
date and place of birth: 06.11.1984, Halle (Germany)

Education:

1991-1995 primary school "Wittekind" Halle
1995-2004 grammar school "Thomas-Müntzer-Gymnasium"
2004 Abitur with "Abitur award" of the DPG
01.08. - 30.09. 2004 internship; "Changing the transmission and polarization of glasses by metallic nanoparticles" at Martin Luther University Halle-Wittenberg
2004-2010 studies of physics at Martin Luther University Halle-Wittenberg; diploma title: "Boltzmann-Gleichung für geladene Teilchen mit Spin" ("Boltzmann equation for charged particles with spin")
01.11.2007-31.03.2010 student research assistant at Martin Luther University Halle-Wittenberg
01.05.2010-31.07.2013 PhD studentship at Max Planck Institute of Microstructure Physics Halle
2012-2013 member of the international Max Planck research school for Science and Technology of Nanostructures in Halle

EIDESSTATTLICHE ERKLÄRUNG

Hiermit bestätige ich gemäß der Promotionsordnung der Naturwissenschaftlichen Fakultät II der Martin-Luther-Universität Halle-Wittenberg vom 13.06.2012, dass ich die vorliegende Arbeit

"Spin Nernst & spin Hall effect in dilute metallic alloys"

selbstständig und ohne fremde Hilfe verfasst, keine außer die angegebenen Quellen und Hilfsmittel benutzt habe und die wörtlich übernommenen Stellen kenntlich gemacht habe. Desweiteren erkläre ich, dass ich die Angaben wahrheitsgemäß gemacht habe und keine Arbeit an einer anderen wissenschaftlichen Einrichtung zur Erlangung eines akademischen Grades eingereicht habe.

Halle, December 13, 2013

Katarina Tauber